International Journal of Mining Science (IJMS)
Volume 6, Issue2, 2020, PP 11-33
ISSN 2454-9460 (Online)
DOI:http://dx.doi.org/10.20431/2454-9460.0602002
www.arcjournals.org

Mineralogical and Geochemical Studies on Kab Amiri Altered Granetic Rocks and Associated Pegmatite, Central Eastern Desert of Egypt

Ahmed M. El Mezayen[1], Ehab K. Abu Zeid[2], Mohamed G. El-Feky[2], Sayed M. Omar[2], Hani H. Ali[2], Sherif A. Taalab[1*]

[1]*Department of Geology, Faculty of Science, Al-Azhar University, P.O. 11884, Nasr City, Cairo, Egypt*

[2]*Geochemical Exploration Department, Nuclear Materials Authority, P.O.530, El-Maadi, Cairo, Egypt*

Corresponding Authors:** ***Sherif A. Taalab, *Department of Geology, Faculty of Science, Al-Azhar University, P.O. 11884, Nasr City, Cairo, Egypt*

Abstract: *The main rock units exposed in Kab Amiri area are chronologically arranged as follows; Dismembered ophiolitic rocks that are represented by serpentinites and talc- carbonates rocks and metabasalts, Island arc assemblage are represented by metasediments and metavolcanics rocks, granitoid rocks include syn orogenic granites, late orogenic granites and episyenite, dikes (aplitic and basaltic), pegmatite and stream sediments. Mineralogical investigations show the presence of fergusonite and columbite as Nb-Ta mineral group, uraninite, thorite, uranothorite and zircon thorite intergrowth as radioactive minerals, zircon, fluorite and allanite as radio- REEs bearing minerals, Field and petrological Pravrach regulation and coordination studies demonstrate that the main alteration features in the studied rocks are hematitization, sericitization, saussuritization, kaolinitization, albitization, chloritization, silicification, and muscovitization. Highly altered granite was confirmed from the unusual ratios of isovalents as Y/Ho, Zr/Hf, Nb/Ta and La/Y. The TREE average in the studied granites and pegmatites is lower than the international values and the granites show enrichment in the LREEs contrasting to pegmatites. Rare earth patterns of granites and pegmatites have complex tetrad effect where they have M-type tetrad associating W-type suggesting severe changes in physico-chemical conditions.*

Keywords: *Radioactive minerals, uraninite, REE-tetrad effect, altered granite, silicification, desilicification, Egypt*

1. INTRODUCTION

Kab Amiri area represents a part of the Central Eastern Desert of Egypt. It can be accessed through Qena-Safaga asphaltic road, at landmark 85 Km from Qena, then through Wadi El-Missikat to Wadi Kab Amiri for about 40 Km on a desert road. It is bounded by Latitudes 26˚ 15` and 26˚ 25` N and Longitudes 33˚ 30` and 33˚ 40` E (Fig. 1). The distribution of isovalent trace element as Y-Ho and Zr-Hf in any geochemical regime depends mainly on ionic radius and charge which are known as CHARAC (charge-radius control). The distribution patterns of these elements are regular mainly resulted from CHARAC attitude that occur during their mobilization (Bau, 1996). Unusual REE pattern that presents during alteration processes could controlled by non-CHARAC (non-charge-radius control) attitude (Monecke et al., 2002). Non-CHARAC attitude of Zr and Hf, Y and Ho didn't clarify only by fractionation of minerals (Bau 1996, 1997).

Many researchers used the term (tetrad effect) which means Zigzag or kinked patterns as Takahashi et al. (2005); Feng, (2010); Lee et al. (2010); Abedini et al. (2017) and Rezaei Azizi et al. (2017). Geochemically, the term Tetrad refers to the subdivision of the 15 lanthanide elements into four groups in a chondrite normalized distribution pattern: (1) the first La–Ce–Pr–Nd, (2) the second Pm–Sm–Eu– Gd, (3) the third Gd- Tb–Dy- Ho and (4) the fourth Er–Tm–Yb–Lu. Gd is the only common lanthanide in the second and third tetrads, and each group forms a smooth convex of REE distribution patterns - so-called convex (M-shaped) and concave (W-shaped) tetrad effects as defined by Masuda et al. (1987). The convex (M-shaped) tetrad effect forms are mainly found in igneous and related systems such as hydrothermal alterations, while the concave (W-shaped) occurs in normalized REE distribution patterns are generally related to low-temperature deposits such as phosphorites,

limestones, marine sediments and cherts as characterized by Akagi et al. (2004); Feng et al. (2014) and Censi et al. (2016). The hydrothermal alteration processes in the acidic rocks are generally accompanied by mineral deposits, especially precious and base metals (Zhang and Smith-Duque, 2014; Watanabe et al., 2018, El Mezayen et al., 2015 and 2019). The present work aims to characterize the least desilicified granites geochemically and minerlogically and deduce the relation between alteration processes and the recorded mineral association.

2. GEOLOGIC SETTING

A 1:50,000 geologic map of the study area was constructed using aerial photographs, Thematic Mapper (Fig. 2). Based on field geologic mapping, mode of occurrence and field relationships; Format the complete bragravers, just like the rest of the research the main rock unites exposed in the Kab Amiri area can be chronologically arranged, from the oldest to youngest, as follows: (1) Dismembered ophiolitic rocks represented by serpentinites, talc- carbonates and metabasalts. Serpentinites and talc- carbonates are gray to grayish-green in color on the weathered surface, moderate to high relief. These serpentinites are intruded by the late orogenic granites to the south of Wadi Kab Amiri with talc-carbonate rocks along the contact and enveloped by metasediments rocks mainly with tectonic contacts (Fig. 3a). Chromite lenses are recognized within the serpentinite rocks. Metabasalts located at the northwestern sector of the studied area. These rocks are characterized by moderately relief with dark gray to greenish gray color and by pillow structures (Fig. 3b). (2) Island arc assemblage include metasediments and metavolcanics. Metasediments are forming a curvilinear belt surrounding the Kab Amiri granite from the south. These rocks are mainly fine to medium grained immature sediments. They are mostly foliated, folded and exhibit grayish green color with moderate to high relief. These rocks show well-developed schistosity (Fig. 3c) and intruded by Kab Amiri granites. Metavolcanics form moderate to high relief ridges with dark gray to greenish gray and pink color. They are highly fractured, altered, sheared and sometime traversed by mafic dikes. The contacts between the metavolcanics and metasediments rocks are structural where as with Kab Amiri granites is sharp structural intrusive contacts. (3) Granitoid rocks include syn orogenic granites, late orogenic granites and episyenite. The syn orogenic granites cropout at both the northwestern and northeastern parts of the mapped area. They intrude the metasediments and metavolcanics rocks with sharp contacts (Fig. 3d). They are coarse-grained and characterized by low to moderate relief, gray color, and obvious planner structure arising mainly from the preferred orientation of mafic minerals. The late orogenic granites are represented in Kab Amiri granite pluton. This pluton is an oval-shaped body with a diameter ranging from 6 to 8 Km and a peak 982 m above sea level. This pluton intrudes the serpentinites (Fig. 3e) with typical intrusive contact. These rock are medium to coarse-grained and distinguished by pink to red color. There are two types of altered granites in the study area, the first is the least desilicified, while the other is the highly desilicified granite (Fig. 3f). The least desilicified granites are represented by the sheared and hydrothermally altered parts from the main pluton of late orogenic granites, especially at the contact with the metasediments associated. The highly desilicified granites (episyenite) are related to the small stock like episyenite body that intrude the metasediments associated. Episyenite crops out at about 1.8 Km from the southern periphery of Kab Amiri granitic

pluton within the metasediments rocks. It shows sharp intrusive contact with the metasediments rocks (Fig. 3g). It shows spongy shape due to dequartizification vugs and mostly radioactive. Pegmatites are found as pockets, lenses or veins along some fault zones. The pegmatite pockets are of variable size ranging from 20 to 30 m in length and from 1 to 15 m in width. They are mainly associated with the late orogenic granites and exhibiting sharp contact (Fig. 3h). Some pegmatite bodies are characterized by containing radioactive mineralizations (Fig. 3i).

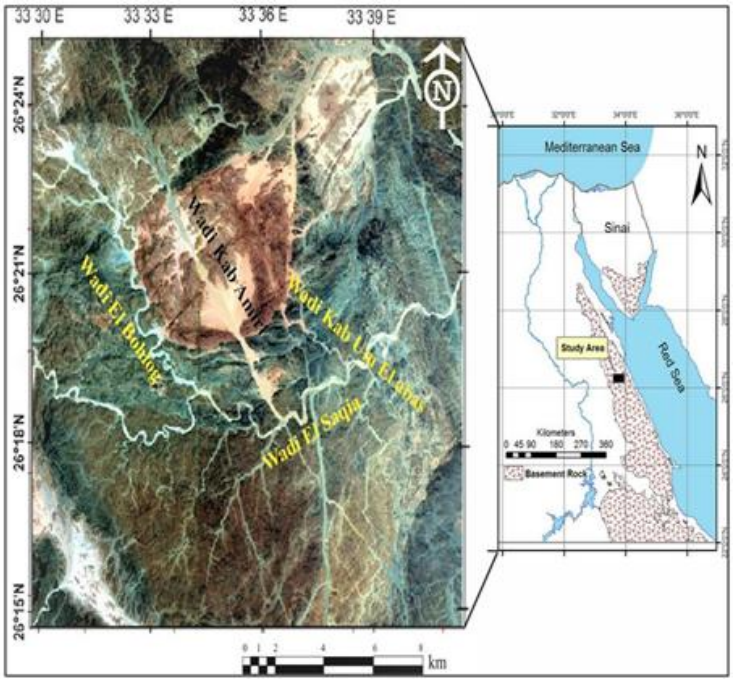

Fig. 1. *Location map and Landsat-7 ETM+ band 7, 4, 2 in R, G, B color channels of Kab Amiri area, Central Eastern Desert, Egypt.*

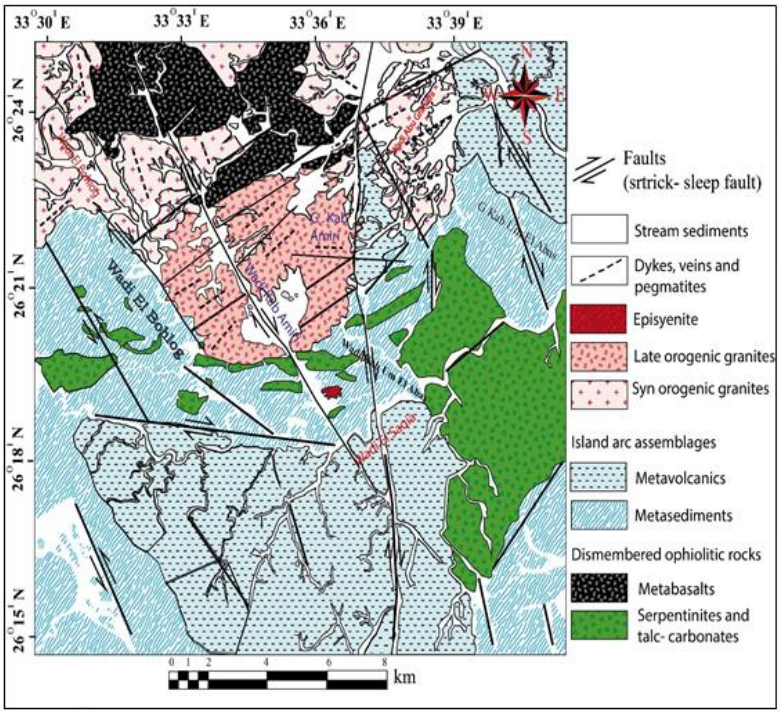

Fig. 2. *Geologic map of Kab Amiri area, Central Eastern Desert, Egypt (modified after Gaafer and Aboelkhair 2014)*

3. Materials and Analytical Methods

Petrographic examinations were carried out on 13 thin sections of altered granites and pegmatites using a polarizing microscope. The samples of altered granite and pegmatite were selected for the separation of their heavy mineral fraction. The collected samples were crushed, ground, quartered and sieved to −60 to +120 meshes size fraction and finally these samples were separated heavy liquids separation technique using bromoform of specific gravity 2.85, gm/cm^3 to concentrate the heavy minerals. Then, the separation of magnetite was achieved by hand magnet. The heavy mineral fractions were passed through a Frantz Isodynamic Magnetic Separator Model L-1, at a side tilt of 5^o and forward slope 20^o, to separate the remaining magnetite and produce several magnetic fractions at 0.2, 0.5, 0.7, 1, and 1.5 amperes. Minerals identification were picked under a binocular microscope and identified using environmental scanning electron microscope (ESEM) supported by EDX and XRD.

The identification of the minerals was carried out by: (1) the X-ray diffraction technique (XRD), using a Philips PW3710/31 diffractometer and scintillation counter, a Cu-target tube and a Ni filter at 40 kV and 30 mA. (2) The environmental scanning electron microscope (ESEM model Philips XL 30) supported by an energy dispersive spectrometer (EDX) unit was used at 25–30 kV accelerating voltage, 1–2 mm beam diameter and 60–120 s counting time. Chemical analyses of whole-rock samples were carried out in ACME Analytical Laboratories Ltd., Vancouver, Canada, for major oxides and trace elements by inductively coupled plasma emission spectrometry (ICP-ES). Rare earth element concentrations of the selected 13 samples were determined by inductively coupled plasma mass spectrometry (ICP-MS) method at the same laboratory (ACME). Detection limits for major oxides and trace elements vary from 0.001 wt.% to 0.04 wt.% and 0.01 to 0.5 ppm respectively. For determination of the LOI (loss on ignition), 1 gram of each sample was heated at 950°C for 90 minutes, and then the weight loss during this process was calculated as LOI.

4. Results

4.1. Petrographically of Altered Granite

According to the petrographic examination, the recorded alteration types affecting Kab Amiri least altered granites are hematitization, sericitization, saussuritization, kaolinitization, albitization, chloritization, silicification and muscovitization.

Sericitization is one of the most common types of hydrothermal alteration found in felsic rocks. In the studied rocks, sericitization is recorded as an alteration product of K-feldspar (microcline) and surrounded by unaltered still reserved marginal parts of microcline (Fig. 4a). Albitization (phyllic alteration) of plagioclase is the decalcification of its anorthite content; this alteration is accompanied by saussuritization of the plagioclase (Fig. 4b). Chloritization occurs in the interstitial spaces between hornblende, plagioclase, biotite and quartz that represent pathways for the altered solutions. The grains within the interstitial spaces are of violet and inexperienced in color (Fig. 4c).

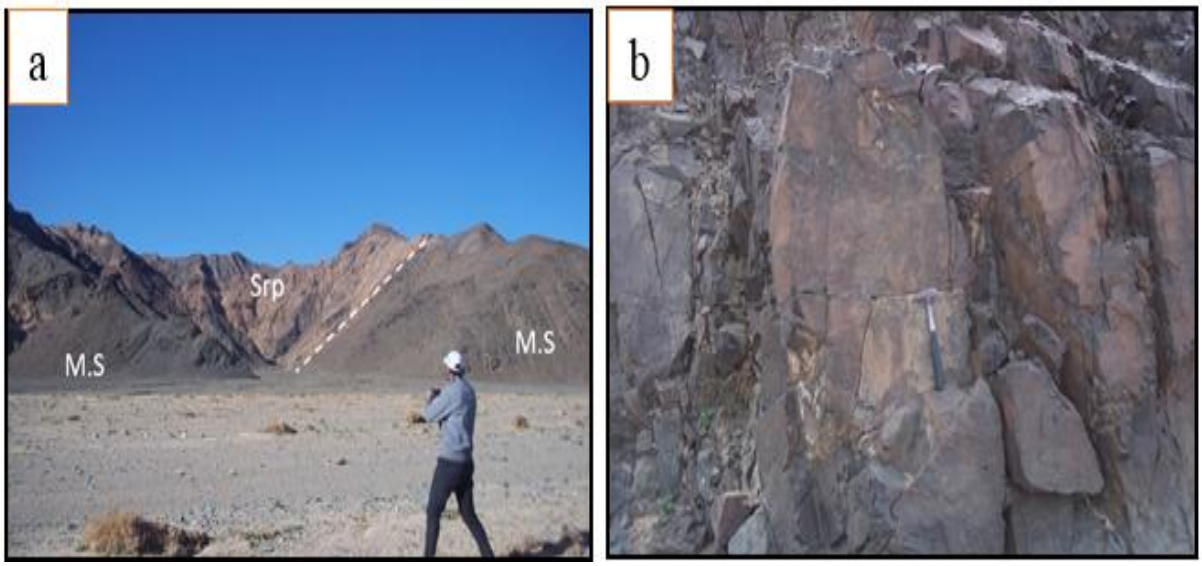

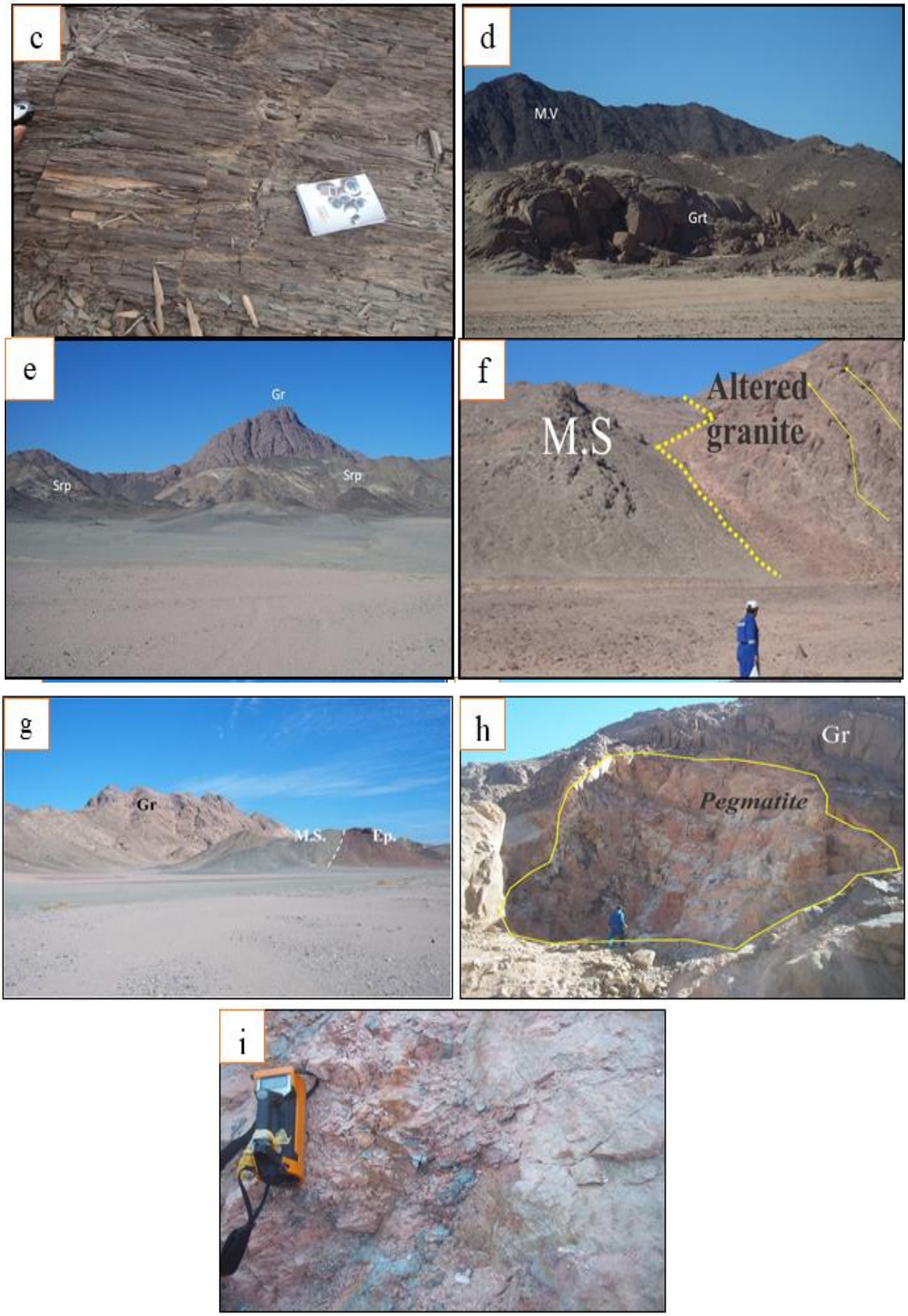

Fig. 3. *Photographs of (a) Tectonic contact between serpentinites (Srp) and metasediments rocks (M.S); (b) Brecciated pillow structure in metabasalts; (c) Schistosity of metasediments rocks; (d) Sharp contact between syn orogenic granite (Grt) and metavolcanics (M.V); (e) Sharp intrusive contact between late orogenic granite (Gr) and serpentinites (Srp); (f) Contact between highly sheared altered granite and metasediments rocks; (g) Episyenite (Ep.) intruding the metasediments rocks (M.S); (h) Quarried pegmatite pocket included in the post orogenic granites; (i) Radioactive mineralization in pegmatite body.*

Changes between biotite and chlorite are commonly occurring in early deuteric alteration and in late hydrothermal alteration. There are two generations of muscovite in the studied altered granites. The primary muscovite is represented by large crystals and the second muscovite is formed at the expense of K-feldspar and represented by small crystals occupying the interstitial spaces between plagioclase and quartz (Fig. 4d). The main accessory minerals in altered granites are zircon, allanite, apatite and opaques minerals (Fig 4(e), (f), (g) and (h)).

4.2. Mineralogical Studies of Altered Granites and Pegmatite

The mineralogical investigation of the studied altered granites and pegmatite is of great importance. The obtained data from both ESEM analyses and X-ray diffraction revealed the presence of the following mineral groups:

4.2.1. Niobium–Tantalum Minerals

4.2.1.1. Fergusonite ($YNbO_4$)

Three types of fergusonite were recorded in the studied altered granites and pegmatite. The first type of fergusonite occurs as rounded to sub rounded grains, with yellowish brown to dark brown color, as confirmed by Environmental Scanning Electron Microscope (ESEM) microphotograph and EDX spectra (Fig. 5a). It is mainly composed of Pb (6.04 Wt. %), Y (8.87 Wt. %) and Nb (29.81 Wt. %). The second type of fergusonite is vacant from Y and Pb as confirmed by (ESEM) (Fig. 5b) and composed of Th (11.71 Wt. %), U (40.58 Wt. %) and Nb (22.58 Wt. %). The third type of fergusonite contains REEs with Th and U. Fergusonite in this type has Nb (40.86 wt.%), Th (9.63 Wt. %), U (9.19 Wt. %), Ce (0.36 wt.%), Gd (2.13 Wt. %), Dy (3.52 Wt. %), Yb (4.63 wt.%) and Y (20.32 wt.%) (Fig. 5c).

4.2.1.2. Columbite [(Fe, Mn, Mg) (Nb, Ta) $2O_6$]

Columbite is an ore of niobium as well as a source of tantalum. It is generally occurring as reddish to dark brown and/or tabular, rounded crystals. The enrichment of columbite in U and Y is also recognized. It is frequently considered as a carrier of radioactivity and also REEs. Columbite, ferrocolumbite and yttrocolumbite grains were recorded in the studied altered granites and pegmatite (Fig 5(d), (e) and (f)). ESEM microphotograph and EDX analyses indicate that ferrocolumbite contains high contents of iron while yttrocolumbite has high amounts of yttrium.

4.2.2. Radioactive Minerals

4.2.2.1. Uraninite (UO_2)

Uraninite is a common accessory mineral in pegmatites and peraluminous granites and is probably the most important source of dissolved U in groundwaters emanating from weathered granite terrains. Uraninite is considered as primary uranium mineral and commonly contains Th, REE, Ca, and other elements. ESEM microphotograph and EDX analyses for uraninite grains are presented in (Fig. 5(g)). It contains U (80.52 Wt. %), Si (10.58 Wt. %), Al (4.53 Wt. %), K (1.53 Wt. %) and Ca (2.45 Wt. %).

4.2.2.2. Uranothorite [(Th, U) SiO_4]

Uranothorite is one of the most common thorium silicate minerals. ESEM microphotograph and EDX spectra for uranothorite grains presented in (Fig. 5(h)) it is mainly composed of Si (20.17 Wt. %), U (23.91 Wt. %), Th (41.46 Wt. %) and Y (11.19 Wt. %).

4.2.2.3. Thorite ($ThSiO_4$)

Thorite occurs as black to brownish black grains and/or rounded to sub rounded grains or prismatic crystals. It is found as an accessory mineral in different rock types and geologic environments, especially pegmatites, granites, quartz barite veins, syenites and hydrothermal deposits. It is considered a primary mineral. Thorite grain is often massive. EDX analyses clarify that this mineral is essentially composed of Si (16.22 Wt. %), U (19.36 Wt. %), Th (49.08 Wt. %) and Y (6.41 Wt. %) (Fig. 5(i)).

4.2.2.4. Zircon-thorite intergrowth

The reacting solution with zircon and other associating minerals xenotime, thorite, uranothorite, xenotime, monazite and other minerals leading to the enrichment of this solution by various elements as Zr, Hf, Th, U and REEs, with different degrees depending

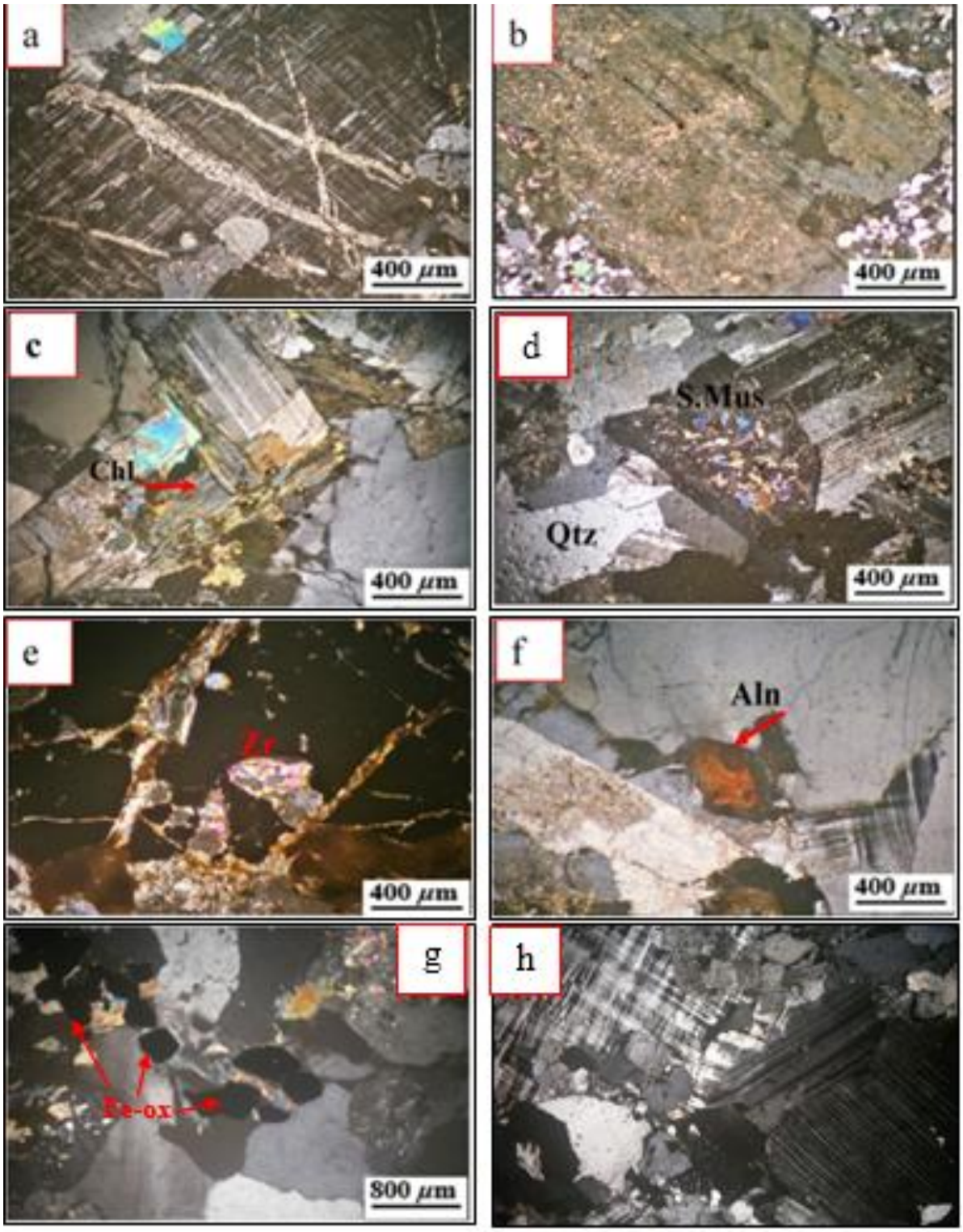

Fig. 4. *Photomicrographs of altered granites showing. (a) Veins of sericite dissecting microcline; (b) Saussuritization of plagioclase; (c) Flake of chlorite crystal (Chl) after biotite; (d) Muscovitization of K-feldspar; (e) Euhedral crystals of zircon (Zr) showing high relief and high interference color; (f) Euhedral crystal of allanite (Aln); (g) Opaques minerals iron oxide (Fe-ox); (h) Large crystal of microcline surrounded by crystals of plagioclase and quartz in pegmatite.*

on the stability of their structures (durability). Förster (2006) reported the presence of intermediate solid solutions in the Th-Y-Zr-U system in evolved and metasomatically altered, P- poor leucogranites of either I- or A-type affinity. Solid solutions with different ranges could be resulted between these minerals and produced zirconian thorite, thorian zircon, yttrian zircon and yttrian thorite.

ESEM microphotograph for zircon- thorite association reflects the chemical composition of zircon and its thorite inclusions as presented in (Fig. 5(j)).

4.2.3. Radio and Rare-Earth Bearing Minerals

4.2.3.1. Zircon ($ZrSiO_4$)

Zircon is a common accessory mineral in plutonic igneous rocks. The metamict state (breakdown of the crystal structure) in zircon may be due at least in part to the presence of radioactive atoms. Under a binocular microscope, zircon occurs as short and long euhedral prismatic crystals, possessing various colors (pale yellow, reddish brown and colorless) and are generally translucent to opaque. Darkening in color of zircon may be attributed to the radiation damage resulting from their contents of Th and U in zircon crystals. The occurrence of U only in zircon crystals indicates secondary hydrothermal metamorphic origin, but not the magmatic origin. ESEM microphotograph and EDX analyses show zircon grain, zircon on K-feldspar, zirconium in grain (Fig. 5(k), (l) and (m)) and mainly composed of Si (31.58, 38.05 and 9.94 Wt. %) and Zr (36.15, 38.77 and 75.94 Wt. %), respectively.

4.2.3.2. Allanite $(Ca, Ce, Y, La)_2 (Al, Fe^{+3})_3(SiO_4)_3(OH)$

Rare earth minerals mainly occur in the fine fraction (<1 mm) and they have different contents of rare earth elements. These minerals are mainly enriched in Ce and Nd, suggesting that they mainly result from thorite dissolution. Allanite occurs in the altered granites as immature allanite crystals (worm like) and suggests an epigenetic nature and consequently a metasomatic origin for some allanite crystals. Allanite may be replaced by thorite during weathering and thorium may be released from allanite and becomes concentrated in secondary phases (Wood and Ricketts, 2000). Two varieties of allanite are known to exist: allanite-(Ce), represented by $(Ce,Ca,Y)_2(Al,Fe^{2+},Fe^{3+})3(SiO_4)_3(OH)$, and the second variety allanite-(Y), represented by $(Y,Ca,Ce)_2(Al,Fe^{2+},Fe^{3+})_3(SiO_4)_3(OH)$ (Scott and Ricketts, 2000). ESEM microphotograph and EDX spectra for allanite grains are present in (Fig. 5(n) and (o)).

4.2.3.3. Fluorite (CaF_2)

Fluorite commonly occurs in hydrothermal pegmatitic, and pneumatolytic veins; in cavities of granites; and occasionally in carbonate rocks and phosphorites (Deer et al., 1992). In the studied rocks, fluorite ranges in color from colorless, blue, pale rose, pale violet to dark violet with anhedral, rounded to subrounded mineral grains. The color variation of fluorite is mostly attributed to the colored impurities and/or radiogenic effects of radioactive materials (El Mansi, 2000; El Mowafy et al., 2007). EDX analyses indicate that it is composed of F (20.0 Wt. %), Ca (77.65 Wt. %) and Y (2.35 Wt. %), (Fig. 5(p)). Another fluorite type was also identified by EDX analysis and it is mainly consisting of F (0.74 Wt. %) and Ca (7.49 Wt. %) as main constituents with Fe (3.75 Wt. %), Si (11.73 Wt. %), Al (4.66 Wt. %), Ta (2.38 Wt. %), U (47.07 Wt. %) and Nb (21.97 Wt. %), (Fig. 5(q)).

4.2.4. Sulphide Minerals

4.2.4.1. Pyrite FeS_2

Pyrite in the study area occurs as pale yellow to brown rounded to subrounded grains. It is the main observed sulphide mineral and considered the source of the widely distributed iron minerals. Environment Scanning Electron Microscope (ESEM) images and EDX spectra microanalyses of pyrite were carried out and illustrated in (Fig. 5(r)). it contains S (55.06 Wt. %) and Fe (44.94 Wt. %).

The results of X-ray diffraction (XRD) analyses show pronounced peaks for Anhydrite and Muscovite, zircon and xenotime, pyrite and fluorite (Fig. 6(a), (b), (c) and (d) respectively) these minerals phases in the altered samples.

4.3. Major Oxide Variations

The concentration values of major oxides in the altered granites and pegmatite samples at Kab Amiri area are listed in (Table 1). The average of SiO_2 content varies within the range of 72.79–76.41 wt.% and from 60.29- 67.70 wt.% in the altered granites and pegmatite samples, respectively. Al_2O_3 and total iron oxides in the altered granites range from 1.94 to 13.28 wt.% (mean 12.6 wt.%), and from

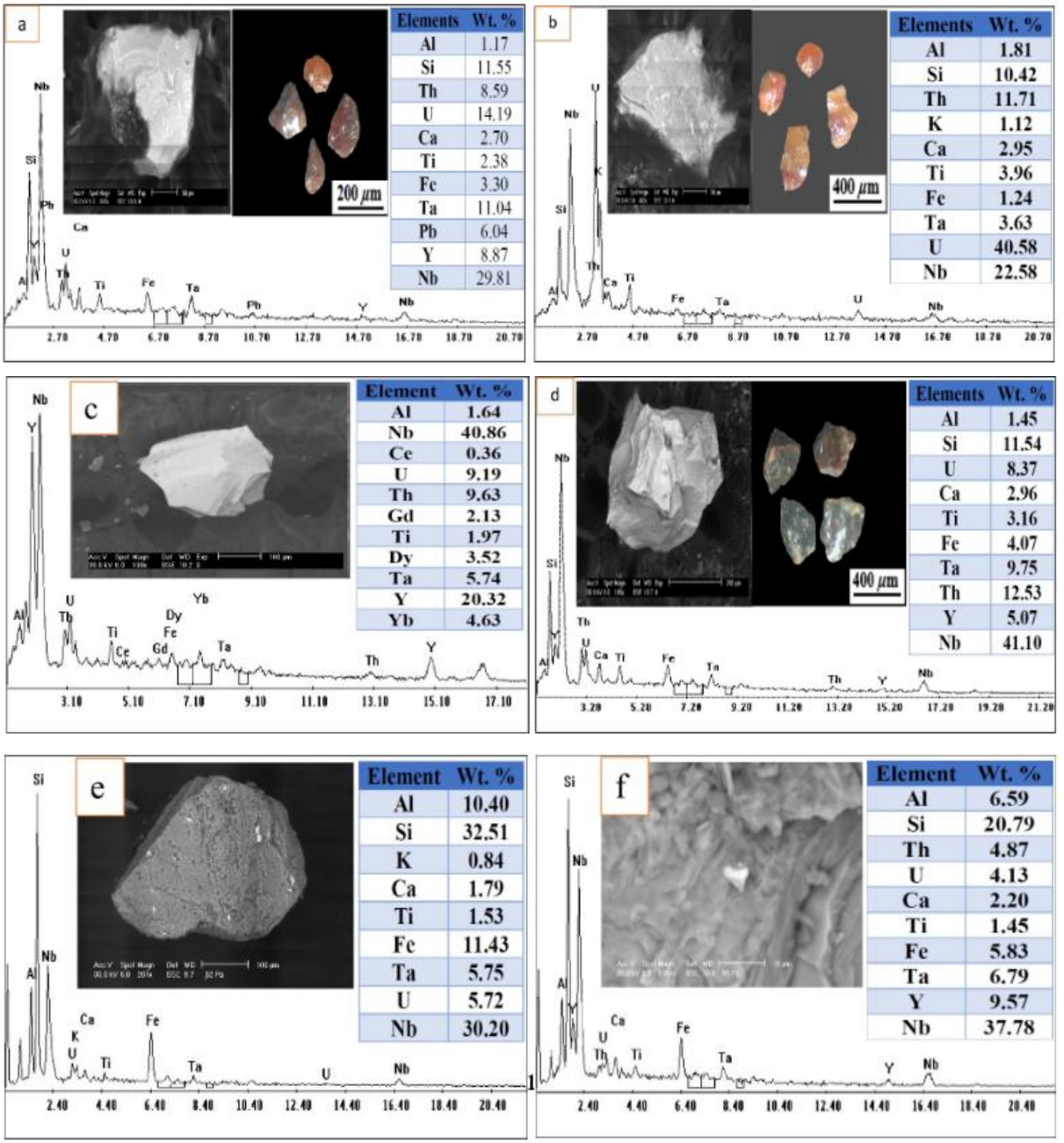

Fig. 5. *Binocular microscope images, Backscattered electron (BSE) images and EDX analysis for (a) Fergusonite mineral; (b) Fergusonite without Y +Pb; (c) Fergusonite with Th, U and REE minerals; (d) Columbite mineral; (e and f) Ferrocolumbite and Yttrocolumbite minerals, respectively.*

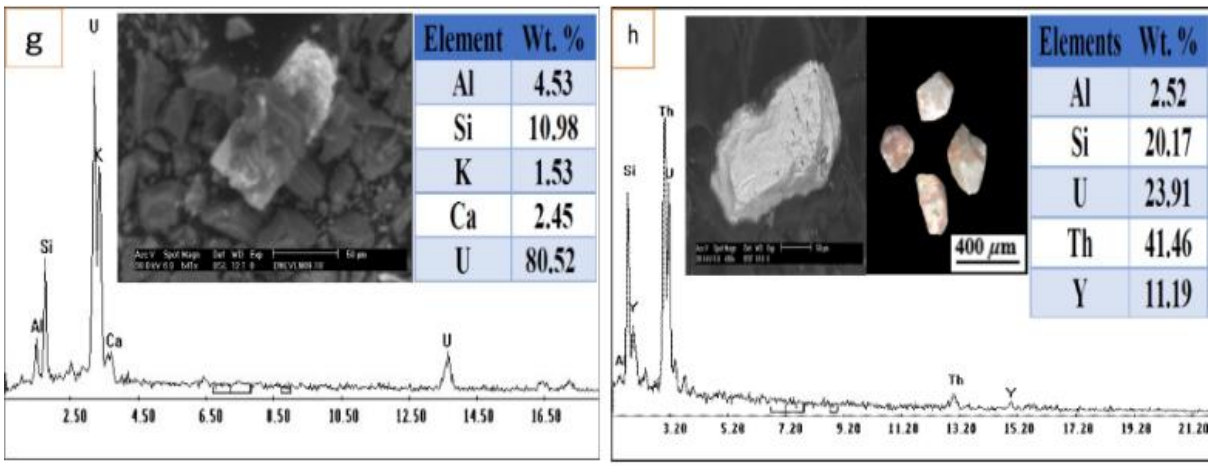

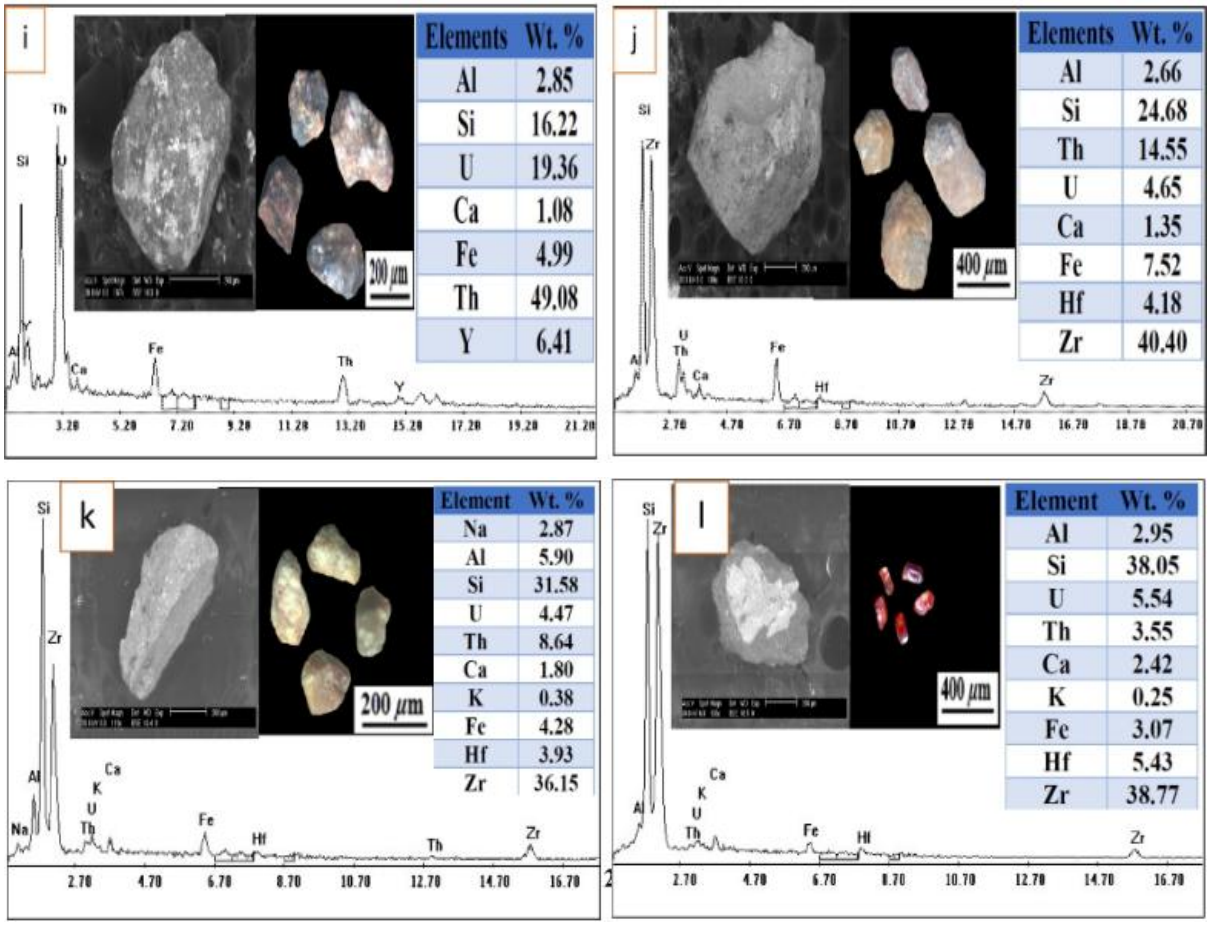

Fig. 5. *Binocular microscope images, BSE images and EDX analysis for (g) Uraninite mineral; (h) Uranothorite mineral; (i) Thorite mineral; (j) Zircon-thorite association; (k) Zircon mineral; (l) Zircon on K-feldspar mineral.*

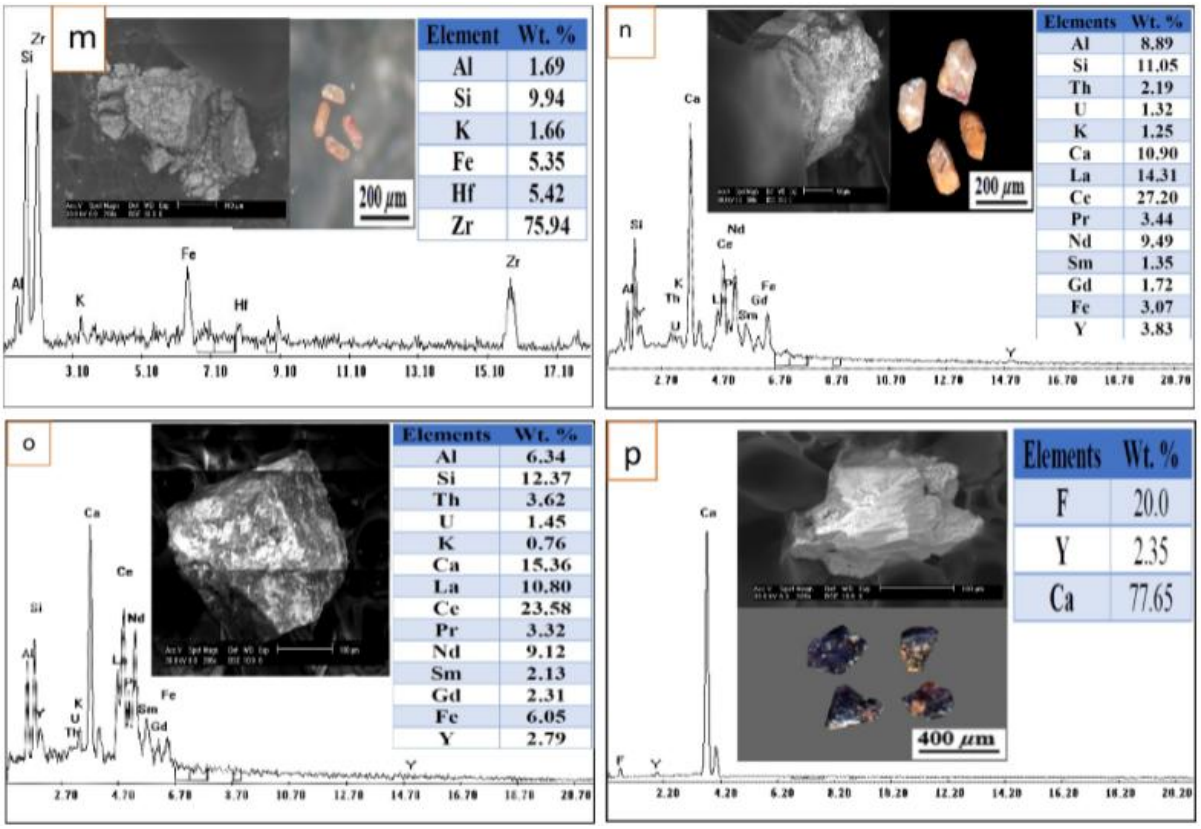

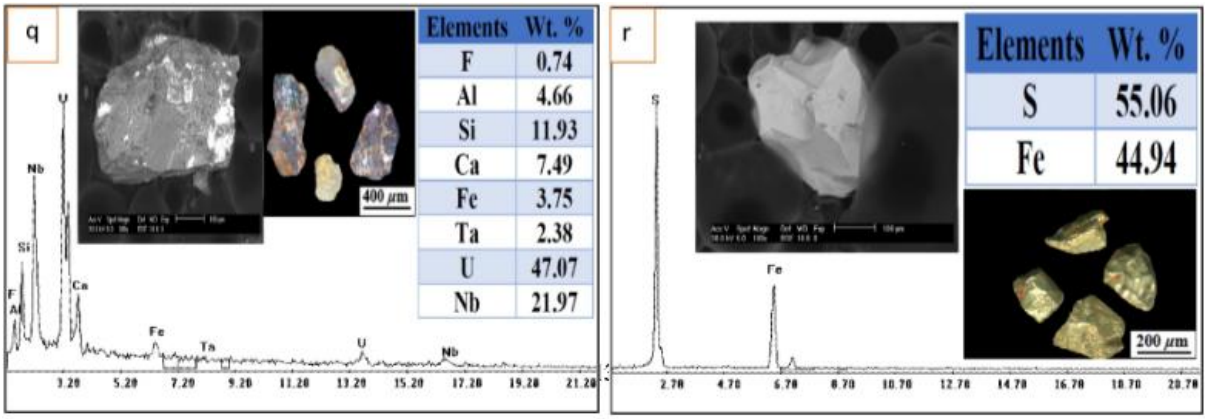

Fig. 5. *Binocular microscope images, BSE images and EDX analysis for (m) Zirconium in grain mineral; (n and o) Allanite mineral; (p and q) Fluorite mineral; (r) Pyrite mineral.*

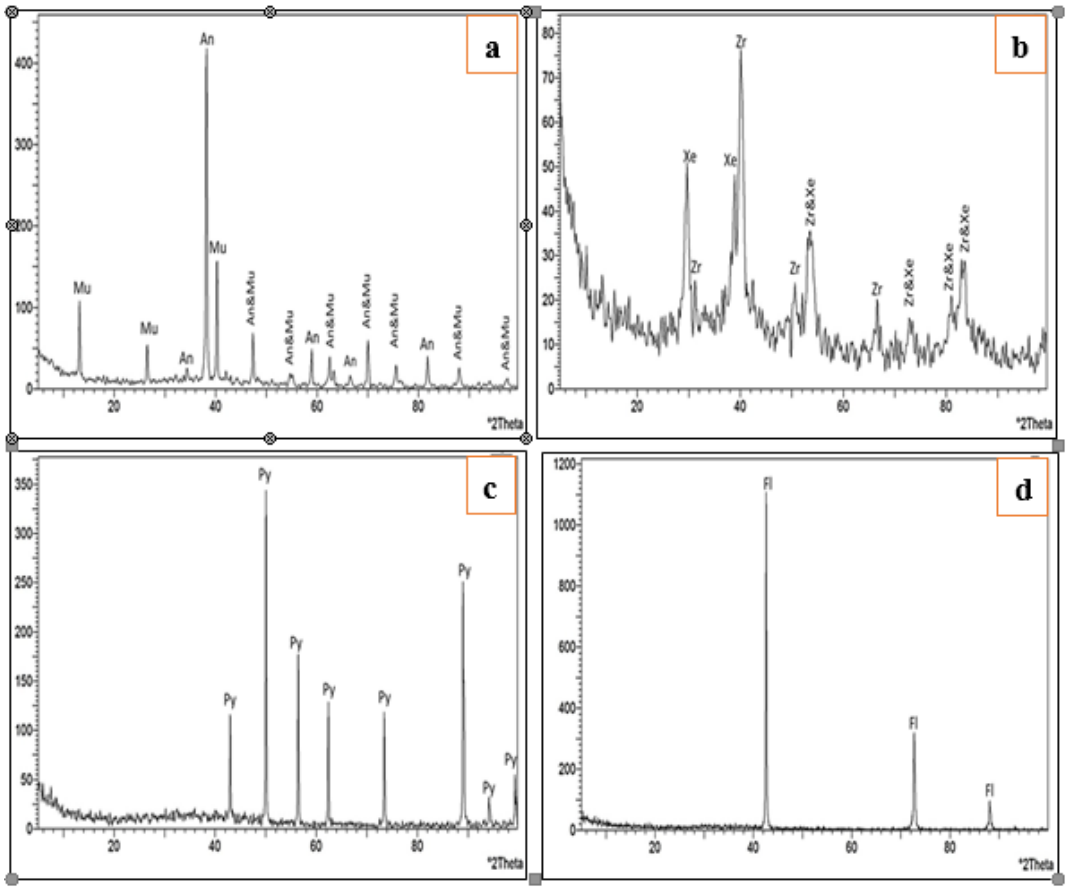

Fig. 6. X-ray diffraction (XRD) patterns for (a) Anhydrite (An) and Muscovite (Mu); (b) Zircon (Zr) and Xenotime (Xe); (c) Pyrite (Py); (d) Fluorite (Fl).

Table 1: Chemical composition of Kab Amiri altered late orogenic granites and pegmatites Central Eastern Desert, Egypt

Rock type	Altered granites										Pegmatites		
S. No.	16 A	20 A	8 B	19 B	3 C	6 C	18 D	1 F	8 D	23 A	9 A	12 A	13 A
Major oxides (wt.%)													
SiO_2	73.47	74.11	72.79	75.19	73.46	76.41	76.30	75.23	76.25	74.78	60.29	67.70	64.56
TiO_2	0.16	0.13	0.13	0.22	0.18	0.08	0.06	0.09	0.09	0.07	0.15	0.00	0.11
Al_2O_3	13.28	13.19	12.70	12.15	12.70	11.94	12.45	12.64	12.09	12.57	17.80	17.53	18.1
$Fe_2O_3^t$	2.55	2.09	2.93	2.25	2.66	1.85	1.01	1.6	1.82	1.11	6.44	0.22	1.02
MnO	0.06	0.02	0.04	0.05	0.05	0.07	0.10	0.04	0.10	0.08	0.09	0.00	0.01

MgO	0.30	0.23	0.23	0.18	0.23	0.10	0.05	0.10	0.08	0.83	0.10	0.03	0.11
CaO	0.74	0.35	1.34	0.84	1.27	0.49	0.64	0.78	0.63	0.69	1.43	0.07	1.23
Na_2O	4.11	4.28	3.91	3.71	3.72	4.18	4.49	3.88	4.00	4.33	7.76	3.21	5.50
K_2O	4.43	4.53	4.77	4.79	4.26	4.47	4.46	4.69	4.72	4.77	4.37	10.95	8.45
P_2O_5	0.04	0.04	0.03	0.02	0.04	0.01	0.00	0.00	0.00	0.00	0.00	0.00	0.00
L.O.I	0.86	1.03	1.13	0.6	1.43	0.4	0.44	0.95	0.22	0.77	1.57	0.29	0.91
Total	100%	100%	100%	100%	100%	100%	100%	100%	100 %	100%	100%	100%	100 %
Trace elements (ppm)													
Mo	1.32	0.15	0.20	0.88	1.83	1.17	4.56	1.75	1.45	2.82	31.40	0.28	29.6
Cu	4.6	3.0	1.5	5.1	1.5	1.1	1.2	1.6	0.7	0.8	3.7	2.4	2.9
Pb	59.19	12.92	21.20	15.51	32.45	97.36	29.83	61.65	29.42	119.75	63.03	48.36	70.3
Zn	46.9	16.6	27.9	42.9	27.5	47.2	44.0	25.7	45.4	66.8	79.0	10.9	66.5
Ag	20	20	21	20	21	20	20	20	20	20	-	156	-
Au	-	-	-	-	-	-	0.39	-	-	-	1.14	-	-
Ni	0.9	1.2	1.0	0.7	1.0	0.8	0.8	0.7	0.7	0.6	0.7	0.7	0.9
Co	1.4	0.8	1.5	0.9	1.6	0.4	0.2	0.4	0.4	0.4	1.2	0.2	0.9
U	15.0	23.3	9.5	12.6	12.5	15.2	9.3	21.7	5.5	14.1	163.6	15.9	159
Th	25.9	39.1	18.4	31.9	19.3	23.4	30.7	31.5	21.4	71.8	255.7	25.3	247
Sr	89	51	84	73	122	24	14.0	30.0	22.0	29	17.0	7.0	14.8
Bi	0.08	0.10	0.04	0.04	0.06	0.05	0.07	0.04	0.04	0.08	1.39	0.30	1.55
V	11.0	8.0	6.0	5.0	11.0	2.0	1.0	2.0	2.0	1.0	1.0	1.0	1.0
Cr	5.0	3.0	10.0	4.0	7.0	7.0	11.0	6.0	5.0	5.0	2.0	1.0	2.6
Ba	331	324	338	313	440	85.0	46.0	141	73.0	63.0	23.0	17.0	20.3
W	0.1	0.2	1.5	0.1	0.2	0.1	0.3	0.6	0.1	0.3	3.7	0.1	4.1
Zr	172.5	95.6	117.6	98.5	52.6	91.2	219	176.9	75.7	83.9	1052.5	116	985.4
Sn	3.3	2.2	1.0	2.1	1.6	2.1	5.2	1.4	2.8	2.3	16.6	0.5	13.2
Y	23.3	14.0	6.1	42.0	17.8	28.6	96.3	13.9	39.6	93.9	309.5	10.4	338.3
Hf	11.04	9.41	7.81	12.03	7.15	14.24	34.05	23.08	13.5	15.6	99.57	75.8	85.0
Li	53.4	5.9	8.0	16.8	9.6	15.8	8.2	4.6	13.5	3.0	4.1	0.4	3.5
Rb	676.2	165.1	502.3	110.4	204.2	141.7	307.7	196.6	185.5	193.9	229.1	1110.7	789.0
Ta	11.7	65.5	54.3	11.2	35.0	29.3	13.7	12.6	11.9	68.3	38.0	10.6	26.3
Nb	69.89	115.87	94.76	55.88	111.12	84.27	78.96	71.64	36.81	88.47	244.91	71.03	189.1
Cs	1.5	1.5	0.5	0.6	0.6	0.7	1.0	0.4	0.7	0.5	1.6	4.0	3.2
Ga	17.66	18.25	14.77	17.20	16.62	19.42	24.39	16.05	20.20	20.43	49.06	37.0	50.2
Tl	0.85	0.77	0.35	0.46	0.43	0.60	1.34	0.39	0.72	0.93	0.93	4.87	2.1
Rare earth elements REEs (ppm)													
La	21.7	31.5	54.0	48.9	27.8	19.4	13.8	55.4	22.6	11.0	2.2	1.0	1.8
Ce	45.26	65.46	109.05	104.08	60.23	50.91	34.45	115.61	55.79	29.28	18.41	1.77	15.4
Pr	5.9	8.3	13.3	13.3	7.7	7.2	5.0	14.0	7.5	4.1	1.2	0.2	0.9
Nd	19.7	26.9	43.2	43.1	26.6	25.9	17.8	47.2	27.3	18.7	5.7	0.6	5.8
Sm	3.9	5.1	7.2	9.4	5.8	6.3	5.5	8.1	7.6	6.4	3.9	0.2	4.2
Eu	0.6	0.5	1.1	1.0	0.7	0.4	0.2	0.7	0.3	0.3	0.1	0.1	0.2
Gd	3.4	3.8	4.1	7.1	5.0	5.4	5.7	4.7	6.2	8.9	7.6	0.3	6.1
Tb	0.7	0.6	0.4	1.4	0.7	0.9	1.4	0.7	1.0	2.0	2.7	0.1	1.65
Dy	3.8	2.2	1.4	7.4	3.3	4.9	10.0	2.5	6.5	13.6	23.5	0.6	20.1
Ho	1.0	0.5	0.2	1.7	0.8	1.0	2.6	0.4	1.5	4.0	7.9	0.2	8.1
Er	2.6	1.5	0.5	4.2	2.0	3.1	9.5	1.2	5.4	13.3	35.8	0.7	40.9
Tm	0.5	0.3	0.1	0.7	0.3	0.5	1.9	0.2	0.9	2.4	8.9	0.2	9.7
Yb	3.6	2.2	0.7	4.3	2.0	3.7	14.0	1.4	6.4	16.4	80.7	1.6	76.5

Lu	0.5	0.4	0.1	0.7	0.3	0.8	2.7	0.3	1.2	2.9	18.1	0.3	19.8
La/Nb	0.31	0.27	0.57	0.87	0.25	0.23	0.17	0.77	0.61	0.12	0.009	1.0	0.009
La/Ta	1.8	0.48	0.99	4.3	0.79	0.66	1.03	4.4	1.9	0.16	0.06	0.9	0.07
La/Lu	43.4	78.75	540	69.9	92.7	24.3	5.1	184.7	18.8	3.8	0.12	3.3	0.09
La/Y	0.9	2.25	8.9	1.2	1.6	0.7	0.1	4.0	0.57	0.12	0.007	0.09	0.005
Sr/Eu	138.3	102	76.4	73	174.3	60	70	42.9	73.3	96.7	170	70	74
Eu/Sm	0.2	0.1	0.2	0.1	0.1	0.1	0.04	0.1	0.03	0.04	0.03	0.5	0.05
Y/Ho	23.3	28	30.5	24.7	22.3	28.6	37.0	34.8	26.4	23.5	39.2	52	41.8
Zr/Hf	15.6	10.2	15.1	8.2	7.4	6.4	6.4	7.7	5.6	5.4	10.8	1.5	11.6
Nb/Ta	6.0	1.8	1.7	5.0	3.2	2.9	5.8	5.7	3.1	1.3	6.4	6.7	7.2
U/Th	0.6	0.6	0.5	0.4	0.7	0.6	0.3	0.7	0.3	0.2	0.6	0.6	0.6
Ba/Sr	3.7	6.4	4.0	4.3	3.6	3.5	3.3	4.7	3.3	787.5	1.4	2.4	1.4
Ba/Rb	0.49	2.0	0.67	2.8	2.15	0.60	0.15	0.72	0.39	0.32	0.10	0.01	0.03
Rb/Sr	7.6	3.2	6.0	1.5	1.7	5.9	22.0	6.6	8.4	6.7	13.8	158.7	53.3
La/Ybn	4.1	9.7	52.1	1.3	1.6	3.5	0.7	26.7	2.0	1.5	1.0	0.7	1.2
Tb/Ybn	0.8	1.2	2.4	1.1	1.0	1.0	0.4	2.1	0.9	1.1	1.1	1.4	1.1
La/Smn	3.5	3.9	4.7	1.1	1.1	1.9	1.6	4.3	0.9	1.1	0.9	1.1	1.2
Gd/Ybn	0.8	1.4	4.7	0.9	0.8	1.2	0.3	2.7	1.0	0.9	0.9	0.8	0.8
Ce/Ce*	1.030	1.047	1.040	1.061	1.051	1.139	1.096	1.052	1.108	1.066	2.913	1.003	2.769
Eu/Eu*	0.5	0.3	0.6	0.4	0.4	0.2	0.1	0.3	0.1	0.1	0.1	1.2	0.5
ΣREE	113.16	149.26	235.38	247.28	143.23	130.41	124.55	252.41	150.19	133.28	216.44	7.87	211.15
LREE	97.06	137.76	227.85	219.78	12.83	110.11	76.75	241.01	121.09	69.78	31.24	3.87	28.3
HREE	16.1	11.5	7.53	27.5	14.4	20.3	47.8	11.4	29.1	63.5	185.2	4.0	182.85
LREE/HREE	6.0	12.0	30.3	8.0	8.9	5.4	1.6	21.1	4.2	1.1	0.2	0.9	0.2
t1	1.115	1.130	1.078	1.143	1.117	1.205	1.181	1.110	1.162	1.078	1.872	1.084	1.625
t3	0.962	0.906	0.950	1.007	0.826	0.983	1.057	1.049	0.909	0.950	1.118	1.087	0.891
TE1..3	1.036	1.012	1.012	1.073	0.961	1.088	1.117	1.079	1.028	1.012	1.447	1.085	1.203
t4	1.220	0.991	0.987	1.034	1.040	0.895	0.952	0.842	0.918	0.987	0.894	1.078	0.992
TE1,4	1.666	1.058	1.031	1.087	1.078	1.039	1.061	0.967	1.033	1.031	1.294	1.081	1.270
CIPW normative minerals													
Qtz	30.3	30.58	28.92	33.36	32.32	33.89	32.06	32.8	34.4	29.19	-	6.89	-
Or	26.05	26.64	28.05	28.17	25.05	26.29	26.23	27.58	27.7	28.05	25.7	64.4	49.69
An	3.41	1.48	3.01	2.35	5.37	0.61	0.64	3.22	1.09	0.77	0.83	0.35	-
Ab	34.75	36.19	33.06	31.37	1.45	35.34	37.96	32.8	33.82	36.61	56.21	27.14	43.53
Di	-	-	2.91	1.41	0.56	1.5	0.92	0.55	0.43	1.11	4.16	-	0.59
Hy	1.6	1.27	0.17	0.34	1.15	1.7	-	0.49	-	-	-	0.16	-
Mt	1.95	1.6	2.24	1.73	2.03	1.41	0.77	122	-	-	4.87	0.17	-
Ilm	0.3	0.25	0.25	0.42	0.34	0.15	0.11	0.17	-	-	0.29	-	-
Ap	0.09	0.09	0.06	0.04	0.09	0.02	-	-	-	-	-	-	-
Crn	0.47	0.7	-	-	-	-	-	-	-	-	-	0.27	-

t1, t3, t4 and t are calculated according to Irber (1999).

1.01 to 2.93 wt.% (mean of 1.98 wt.%), respectively. These oxides in the pegmatite samples are within the range of 17.53–18.1 wt.% (mean 17.81 wt.%) and 0.22–6.44 wt.% (mean 2.56 wt.%), respectively. The average of TiO_2 content is very low and varies within the range of 0.06 – 0.22 wt.% and 0.00 – 0.15 wt.% in the altered granites and pegmatites, respectively. The concentrations of CaO,

Na_2O, MgO and K_2O in the altered granites show ranges of 0.35–1.34 wt.%, 3.71– 4.49 wt.%, 0.05–0.83 wt.%, and 4.26–4.79 wt.%, respectively. Meanwhile, the corresponding values in the pegmatites have ranges of 0.07–1.43 wt.%, 3.21–7.76 wt.%, 0.03–0.11 wt.%, and 4.37–10.95 wt.%, respectively. MnO and P_2O_5 have low concentration values in altered granite and pegmatite samples. Finally, the LOI values of all samples vary from 0.22 to 1.57 wt.%.

4.4. Trace/Rare Earth Element Variations and Geochemical Ratios

Trace and REE element values with their elemental ratios are registered in (Table 1). Y, Zr, Ta, Nb, and Hf concentration values in the altered granite samples vary within the range of 6.1–96.3 ppm (mean 37.6 ppm), 52.6–219 ppm (mean 118.4 ppm), 11.2–68.3 ppm (mean 33.2 ppm), 36.81–115.87 ppm (mean 80.8 ppm), and 7.15- 34.05 ppm (mean 14.8 ppm), respectively. On the other hand, the concentrations values for the pegmatite samples vary within the range of 10.4–338.3 ppm (mean 219.4 ppm), 116–1052.5 ppm (mean 717.96 ppm), 10.6–38.0 ppm (mean 24.96 ppm), 71.03–244.91 ppm (mean 168.3 ppm), and 75.8- 99.57 ppm (mean 86.8 ppm), respectively.

The concentrations of U, Th, Sr, Ba and Rb in the altered granites, range from 5.5–23.3 ppm (mean 13.9 ppm), 18.4–71.8 ppm (mean 31.3 ppm), 14.0–122.0 ppm (mean 53.8 ppm), 46.0 – 440.0 ppm (mean 215.4 ppm), and 110.4- 676.2 ppm (mean 268.3 ppm) respectively. While the concentration values for the pegmatite samples vary within the range of 15.9–163.6 ppm (mean 112.8 ppm), 25.3–255.7 ppm (mean 176.0 ppm), 7.0–17.0 ppm (mean 12.9 ppm), 17.0–23.0 ppm (mean 20.1 ppm), and 229.1- 1110.7 ppm (mean 709.6 ppm) respectively. Meanwhile, the ΣREE concentration of the altered granite and pegmatite samples are relatively low and vary from 113.16 to 252.41 ppm and 7.87 to 216.44 ppm. The average of the total REEs content of the studied altered granite and pegmatite (av. ΣREE=167.9 and 145.1 ppm, respectively) which are lower than that of the world wide granite (ΣREE=250−270 ppm) as given by Hermann (1970). The depletion of REEs has been attributed to various processes including magmatic differentiation (Cuney and Friedrich, 1987), hydrothermal leaching (Cathelineau, 1987, El mezayen et al., 2015) and or a combination of both. ΣLREE and ΣHREE concentration values for the altered granite samples are within the range of 12.83–241.01 ppm and 11.4 – 63.5 ppm, respectively, while the concentration values for the pegmatite samples vary within the range of 3.87–31.24 ppm and 4.0 –185.2 ppm, respectively. Meanwhile, the La/Lu ratios for the altered granite and pegmatite samples vary from 5.1 – 540 and 0.12 – 3.3, respectively. The Nb/Ta ratios of the altered granites and pegmatite samples vary from 1.3 to 6.0 and from 6.4 to 7.2, respectively. The Zr/Hf ratios of the altered granite and pegmatite samples vary from 5.4 to 15.6 and from 1.5 to 11.6, respectively.

5. DISCUSSION

5.1. Geochemical Characteristics of the Altered Granites and Pegmatite

The distribution of the trace and REE elements in the altered zones and pegmatites (Table 1) yielded useful information on rock/fluid interaction characteristics, in addition to the physicochemical conditions of the system. During the hydrothermal alteration, nearly all the trace elements were mobilized due to dissolution or replacement of the main components and accessory minerals and new formation of mineral phases. The different types of hydrothermal alterations could be obtained using the normative Qz-Ab-Or of Stemprok (1979) and Na_2O-K_2O variation diagrams (Cuney and Friedrich, 1987). According to the normative Qz-Ab-Or composition, the altered rock samples could be classified into sodic, potassic, silicic and greisen (Fig. 7a). The studied altered granites samples have high SiO_2 content and shifted towards quartz, also show imprints of greizenization with some tendency towards Na-metasomatism as indicated by Manning (1981). On the other hand, pegmatite samples are shifted towards both Na- and K- metasomatism resulting from the enrichment in Na and K. The ternary minimum for 1 kb H_2O pressure from Tuttle and Bowen (1958) and the stars represent the ternary minima for a granite system with 0% and 4% F (Manning, 1981). He shows the migration of ternary minima as F content increases in the melt. The trends of granitic alteration types are from Stemprok (1979). However, other samples with high Na_2O contents are shifted towards albite which is consistent with the enrichment direction of fluorine. During Na-metasomatism, albitization proceeds through the replacement of Na^+ for K^+ and Ca_2^+ of the pre-existing feldspars but silicification results in an increase of SiO_2 at the expense of other major oxides and accompanied with an increase of some trace elements such as Zr, Ba, and Rb. Using the Na_2O- K_2O variation diagram (Cuney, and

Friedrich, 1987), it is evident that the studied altered granites fall in the Na-metasomatism field while pegmatite samples show indications of desilicification, albitization and K-metasomatism (Fig. 7b). Meyer and Hemley (1967) classified the K-silicate facies as: (1) propylitic (containing epidote and chlorite alteration), (2) sericitic (containing plagioclases and K-feldspars, both of which were converted to sericite and (3) potassic (characterized by the alteration of plagioclase into K-feldspar or mafic minerals into muscovite) subtypes. Altered granite and pegmatite samples are plotted on the diagram of Meyer and Hemley (1967) (Fig. 7c). It is evident that most of the samples fall in sericite facies (due to sericitization processes) and the other samples are close to the Al_2O_3-Na_2O+K_2O line, because of their high contents of Al_2O_3+Na_2O+K_2O. On the (Na_2O+CaO) −Al_2O_3−K_2O ternary diagram of Nasbitt and Young (1989) all altered granites and pegmatite samples plot parallel to advanced weathering trend, where its initial trend is parallel to the K_2O−Al_2O_3 side line of the diagram (Fig. 7d)).

5.2. Depletion- Enrichment of Major Oxides, Trace and Rare Earth Elements in the Altered Granite and Pegmatite

The variations in the geochemical characteristics of the altered granites are mainly caused by the loss and gain of some elements. To understand the geochemical behavior of elements in the altered granites, it is recommended to normalize the pattern of such altered rocks to its corresponding fresh granites. After that, the reference granite pattern becomes flat at unity and the relative depletion or enrichment are given by the deviations on both sides of the reference line (Fig. 8,9). Geochemistry of major oxide is discussed in terms of gains (positive) and losses (negative) of these elements during the alteration of granites. Altered samples which are affected by desilicification and hematitization exhibit increase in TiO_2, $Fe_2O_3^t$, Al_2O_3, Na_2O, MgO, CaO. The increase of TiO_2 is mainly related to the presence of titanite and ilmenite. Si mass loss indicates kaolinization of feldspars in the studied rocks. Investigations of lithophile trace elements such as MnO, P_2O_5 and K_2O and a prominent decrease in SiO_2 (Fig. 8a). Enrichment of $Fe_2O_3^t$ may be due to alteration of biotite (chloritization) and hematitization. K_2O gain may result from kaolinitization or sericitization of K-feldspar. Trace elements such as Y, Zr, Nb, Ta, and REEs in different rock types and environments are very important in the deposit geochemistry and Earth evolution as recorded by Rezaei Azizi et al. (2017). The dissolution of minerals during hydrothermal alteration may lead to mobilization of most trace elements and the formation of new mineral phases (El-Mezayen et al., 2015). The trace elements in the altered granite samples show enrichment in Cs, Ga, Nb, Rb, Sr, Ta, Th, U, Tl, V, W, Zr, Sn, Hf, Ba, Pb, Zn and

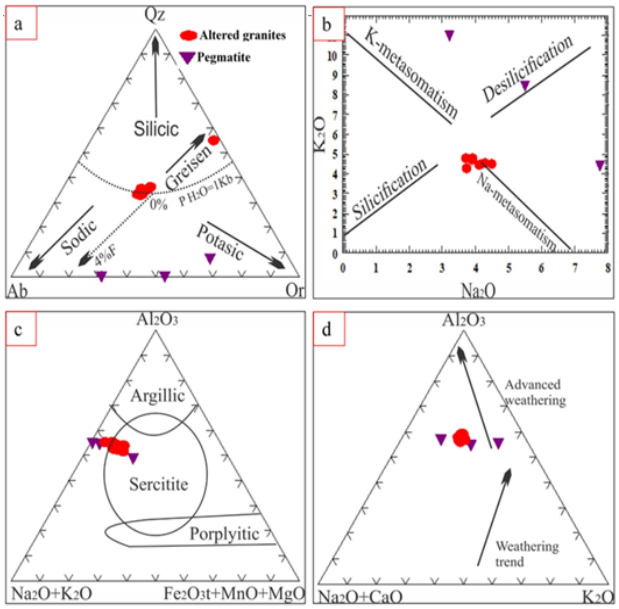

Fig. 7. *Bivariate and ternary diagrams showing. (a) Normative Qz-Ab-Or ternary diagram (**Stemprok ,1979**); (b) K_2O−Na_2O variation diagram (Cuney and Friedrich, 1987); (c) Al_2O_3 − (Na_2O+K_2O) − ($Fe_2O_3^t$+MnO+MgO) ternary diagram (Meyer and Hemly, 1967); (d) (Na_2O+CaO) −Al2O3−K2O ternary diagram (Nasbitt and Young, 1989).*

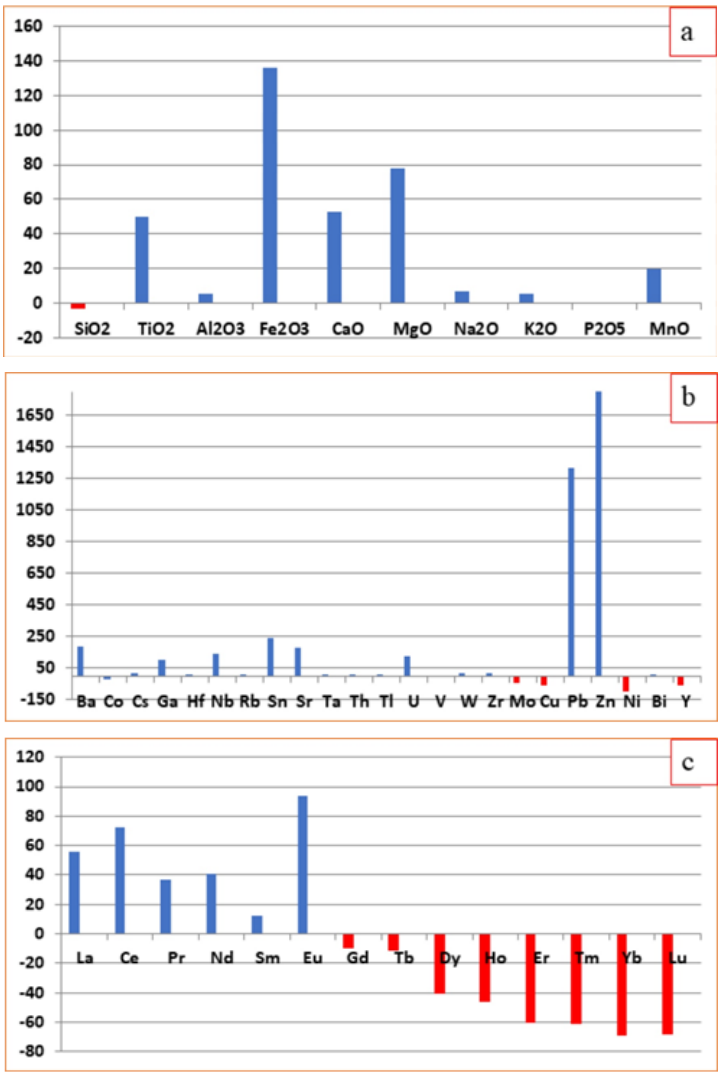

Fig. 8. *Histogram showing the depletion and enrichment of (a) Major oxides of altered granites; (b) Trace elements of altered granites; (c) Rare earth elements of altered granites.*

Fig. 9. *Histogram showing the depletion and enrichment of (a) Major oxides of pegmatites; (b) Trace elements of pegmatites; (c) Rare earth elements of pegmatites.*

Bi, whereas they are depleted in Co, Mo, Cu, Ni and Y (Fig. 8b). However, REEs in the altered granites samples show enrichment in LREEs (La, Ce, Pr, Nd, Sm and Eu) whereas they are depleted in HREEs (Gd, Tb, Dy, Ho, Er, Tm, Yb and Lu), (Fig. 8c). On the other hand, pegmatite samples show an increase in TiO_2, Al_2O_3, CaO, $Fe_2O_3^t$, Na_2O, and K_2O and a decrease in SiO_2, MnO, MgO and P_2O_5. The enhanced Na_2O contents may result from the fact that solutions causing alteration processes are rich in Na_2O (Fig. 9a). The mass loss of Mg and Mn may result from the destruction and alteration of ferromagnesian minerals. Trace elements in the pegmatite samples are either increased as Sn, Hf, Mo, Cs, Ga, Nb, Rb, Ta, Th, U, Tl, W, Zr, Pb, Y, Zn and Bi or decrease of as Ba, Co, Cu, Sr, V, and Ni (Fig. 9b). The chloritization of biotite can probably account for the depletion of Cu and Sr. In contrast to altered granites, the pegmatite samples show enrichment in HREEs (Tb, Dy, Ho, Er, Gd, Tm, Yb and Lu) and depletion in LREEs (La, Ce, Pr, Nd, Sm and Eu), (Fig. 9c). The enrichment in trace elements could be attributed to the presence of radio and accessory minerals as mentioned later.

5.3. Rare Earth Element Tetrad Effect Phenomenon

The values of the tetrad effect were calculated according to the quantification method proposed for quantification of the third and fourth tetrads of Irber (1999): t1 = (Ce/Ce*× Pr/ Pr*), t3 = (Tb/Tb*×Dy/Dy*), t4 = (Tm/Tm* ×Yb/Yb*)

Degree of the tetrad effect T1,3 = (t1 × t3) 0.5. REE pattern that does not show a tetrad effect has values of TE1.3 < 1.1. The M-shaped pattern shows TEi <1.1 and the W-shaped TEi < 0.9.

The REEs tetrad effect is most visible in late magmatic differentiates with strong hydrothermal interactions or deuteric alteration. This includes highly evolved leucogranites, pegmatites and mineralized granites. Moreover, the tetrad effect is often accompanied by other modified geochemical behavior of many trace elements, which is termed by Bau (1996) as non-CHARAC behavior (CHARAC =Charge-and-Radius-Controlled). Such behavior occurs typically in highly evolved magmatic systems enriched in H_2O, CO_2, and elements such as Li, B, F and/or Cl, which suggests the increasing importance of an aqueous-like fluid system during the final stages of granite crystallization (Irber, 1999). According to Masuda et al. (1987), extraction of a coexisting fluid from a peraluminous melt would result in both M-shaped and W-shaped REE tetrad effect, the former of which would be shown in the residual melt phase and the latter of which is shown in the fluid. However, this corresponding relationship for a magma system has not been observed in the natural environment. Recently, it has been argued that peraluminous magmatic systems represent the transition from a silicate melt to a high-temperature hydrothermal system, and thus, the geochemical behavior of the isovalent incompatible elements in highly evolved granitic rocks are controlled mainly by chemical complexation with a variety of ligands (Bau, 1996, 1997). Therefore, the origin of the REE tetrad effect was ascribed to the interaction between fluorine bearing fluid and silicate melt phases (e.g., see Irber, 1999).

Monecke et al. (2002) thought that the convex tetrad effect in the samples from the magmatic environment could not be explained by the removal of a respective complementary REE pattern by a coexisting hydrothermal fluid, as they found that the fluorite samples collected from hydrothermal vein within the end contact of the Li-F granite of Zinnwald, Germany, obviously have the M-shaped REE tetrad effect instead of the W-shaped tetrad effect. Therefore, they proposed that the tetrad effect might have formed within the magma fluid system before emplacement in the subvolcanic environment where phase separation caused a split of this system into fluid and magma subsystems, or that the tetrad effect might also be inherited from an external fluid influencing the system during or after the emplacement of the magma. Takahashi et al. (2002) recently found both W- and M-type tetrad effect in REE patterns for the water rock systems in the Tono uranium deposit, Central Japan, which is interpreted as that the preference of the groundwater for a W-type tetrad effect produces an M-type tetrad effect in the granitic rocks during weathering processes. Cao et al. (2013) stated that the tetrad effect observed in apatite from the muscovite granite and the pegmatite zones of Koktokay No. 3 pegmatite are most likely produced by the interaction of immiscible fluoride and silicate melts, rather than by weathering, fractional crystallization of individual mineral phases and/or fluid melt interaction. Many researchers registered the Co-existence of convex (M-shaped) and concave (W-shaped) tetrad effects in many localities around the world as Qahr-Abad fluorite deposit in Iran (Rezaei Azizi et al., 2017), Terra Rossa in China (Feng et al., 2011), Ti-rich bauxites in Iran (Abedini

et al., 2018), El Sela in the South Eastern Desert of Egypt, Gattar in the northern part of Eastern Desert (El-Feky, 2011) and the studied area . Kawabe et al. (1999), Feng et al., (2011) and El Mezayen et al. (2019) ascribed these phenomena to weathering, alteration and/or fluid or solution mixing. It is important to notice that the reported cases are M- or W-type tetrad effects occurring separately in natural systems. However, the composite M- and W-type REE tetrad effect were firstly reported by ZHAO et al. (2008). Thus, our study is an important step in understanding the REE tetrad effect.

5.4. Geochemistry of Isovalents

The tetrad effect is often accompanied by other modified geochemical behaviors of many trace elements, which is termed by Bau (1996) as non-CHARAC behavior. This means that irregular normalized distribution patterns can be attributed to non-CHARAC behavior of lanthanides during geochemical processes which cause them to be partitioned into four different groups (Monecke et al., 2002). Such behavior occurs typically in highly evolved magmatic systems which are rich in H_2O, CO_2, and elements such as Li, B, F and/or Cl, and which may be regarded as transitional between a pure silicate melt and an aqueous fluid (e.g., London, 1987; Bau, 1996). Zr and Hf are known to have very similar geochemical behavior, which results in a small range of ratios in geological materials. In most igneous rocks, Zr/Hf ratios fall in a narrow range of 33–40. Deviation from the range is rare and usually attributed to metasomatism or intense fractionation of accessory minerals. Zr/Hf ratios of the altered granites range from 5.4 to15.6 and in pegmatites between 1.5 and 11.6 which is to a great extent lower than the normal ratio of geological materials (Granites have Zr/Hf ratio ‹20) suggesting that they are affected by strong magmatic hydrothermal alteration (Irber, 1999; Tang et al., 2014; Rezaei Azizi et al., 2017). Samples showing tetrad effect also have Y/Ho ratio discrepant from the chondritic value (Y/Ho = 28.8) (Zhang et al., 1994; Bau, 1996). The complexation with fluorine is interpreted as a major cause for Y/Ho >28, while the complexation with bicarbonate is assumed to generate Y/Ho values <28. The studied Y/Ho ratios are greatly variable. In the studied altered granites and pegmatite Y/Ho ratios are sometimes chondritic and either higher or lower than the chondritic values suggesting affecting of these rocks by various stages of fluorine or bicarbonate hydrothermal alteration solutions as indicated in the mineralogical studies (Fig. 10).

Nb/Ta ratios of the altered granites and pegmatites are non-chondritic (1.3- 6.0 for altered granite and 6.4 -7.2 for pegmatites). La/ Nb and La/ Ta ratios are (0.12–0.87 and 0.009–1.0), (0.16–4.4 and 0.06–0.9) for altered granite and pegmatites, respectively. The chondritic ratios are 17.6 ±1 for Nb/Ta, (0.96-1) for La/Nb and (16-18) for La/Ta (Jahn et al., 2001). These non-chondritic ratios are considered as another evidence for the highly differentiated nature of the studied altered granites and pegmatites. Rb/Sr ratio increases with differentiation; this is due to the fact that Sr is depleted in the liquid magma as a result of crystallization of feldspar, while Rb is enriched in the liquid phase. The studied altered granites and pegmatites have Rb/Sr ratios (1.5-22.0 and 13.8-158.7, respectively) suggesting Sr enrichment during albitization and for saussuritization. La/Y ratios are higher or lesser than one in the altered granite suggesting the presence of alkaline and acidic environment, whereas pegmatite ratios lesser than one displaying acidic one. A positive correlation between chemically analyzed uranium and thorium of the studied altered granites and pegmatites indicates uranium enrichment with differentiation (Fig.11). Additionally, albitization promoted subsequent fluid circulation (for U, REE and HFSEs) by creating a more brittle and permeable rock assemblage (Alexandre, 2010). The relatively high average of uranium and thorium contents when compared with the crustal values of 1.80 ppm U and 7.20 ppm Th (Mason and Moore, 1991) indicate the increase of these elements in Kab Amiri granites (Fig. 12).

5.5. Rare Earth Elements Geochemistry

In altered granites, there is a drastic decrease in the REE in general where ΣREE 113.16 – 252.41 ppm (Table 1), but Σ LREE 12.83 – 241.01 ppm is higher than Σ HREE 7.53 - 47.8 ppm and Σ LREE / Σ HREE 1.1–30.3. The fractionation of the REE, in general, is high La/Yb (0.7–52.1). It is known that the La/Yb ranges between (30 and 80) for metaluminous granites and between 1 and 9 for

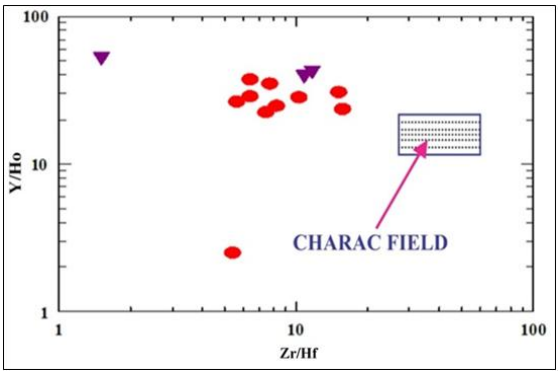

Fig. 10. *Binary diagram of Zr/Hf versus Y/Ho for samples of the altered granites and pegmatites.*

The Charac field is from Bau (1996). Symbols are the same as in Fig. 7.

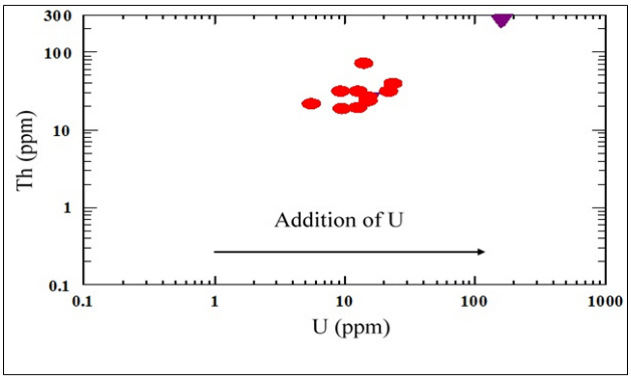

Fig. 11. *Chemically analyzed uranium vs. chemically analyzed Th of the altered granites and pegmatites* ***(Alexandre, 2010****). Symbols are the same as in Fig. 7.*

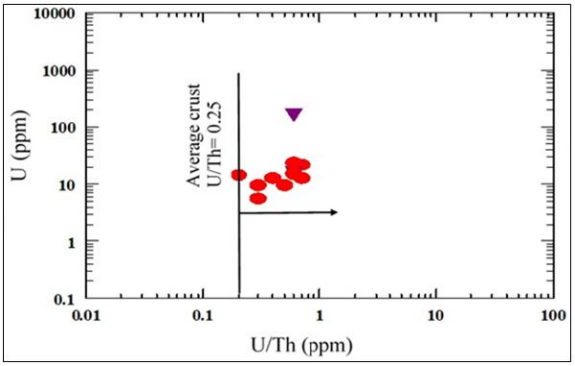

Fig. 12. *U vs U/Th plot showing the enrichment of uranium in the granite of Kab Amiri (Mason & Moore, 1991). Symbols are the same as in Fig. 7.*

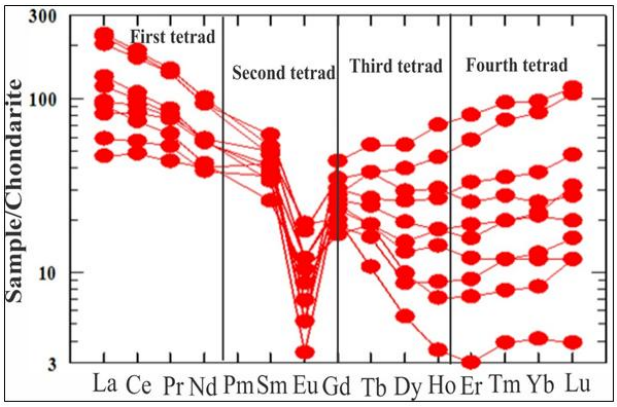

Fig. 13. *Chondrite normalized REE diagram (****Boynton, 1984****) for the investigated of altered granites. Symbols are the same as in Fig. 7.*

peralkaline granites (Harris and Marriner, 1980). The LREEs (La/Sm= 1.1– 4.7) and the HREEs (Gd/Yb= 0.3 to 4.7) are moderately fractionated. A negative Eu anomaly characterizes this granite where Eu/Eu* (0.1-0.6) and Eu/Sm (0.1-0.2). The fractionation among Eu and neighboring REEs (Sm and Gd) with the tetrad effect possibly leads to the decrease in the magnitude of the negative Eu anomaly (Feng, 2010; Ibrahim et al., 2015). The LREE are depleted and the HREE (Gd to Lu) including that Eu and Y are enriched. This general shift towards lower LREE/HREE is only observed in altered granites that underwent albitization. The studied altered granites represent a particular pattern of the rare earth chondrite- normalized elements (**Fig. 13**). A composite M- with W-type of REE tetrad effect is recorded as phenomena previously recorded in China (ZHAO et al., 2008 and 2010; Cao et al., 2013). The kinking in the REE patterns are camouflaged by prominent convex and concave tetrads and pronounced negative Eu anomalies. Visual inspection suggests that the first tetrad in most samples is more prominent than the third and fourth curved segments. The second tetrad is comparably difficult to recognize due to the anomalous behavior of Eu and the fact that Pm does not occur in nature. Figures 13 shows that the samples of altered granites have strong M-type tetrad effect in the first and fourth tetrad and strong W-type tetrad effect in the third tetrad. The index of tetrad effect intensity, TE1,4 average, is higher than 1.10 and ranging from 0.967 to 1.67 in the altered granites, which implies that there was an interaction between the melt and water haloid rich fluid when these granites are crystallized from magma. However, most of the pegmatite samples show clear convex (M-type) with concave (W-type) tetrad effect except one sample shows convex (M-type) tetrad (**Fig. 14** & Table 1). TE1,4 average, is higher than 1.10 and ranging from 1.08 to 1.29 in the pegmatites. ZHAO et al. (2008) suggest that the new MW-type of tetrad effect is likely to be caused mainly by the interaction of aqueous liquids with alkaline rocks. Mahdy and El Kammar, (2003) in Kab Amiri granite, CED, Egypt revised the convex (M-type) T1 accompanying with concave (W-type) T3 to the physicochemical conditions that prevailed during the alkali metasomatism of the Kab Amiri granitoids. ZHAO et al. (2010) and El Mezayen et al. (2015) stated that the peculiar MW-type tetrad effect might be an indicator for Au mineralization of reworked plutons and this vision could be applied in the study area where there are high Ag and Au contents in the altered granite comparing with the fresh one as indicated in (Table 1). Gold and silver reach up to (0.39 and 21 ppm, respectively) in younger granites where pegmatite has higher values (1.39 and 156 ppm, respectively).

6. CONCLUSION

Kab Amiri area is mainly covered by Dismembered ophiolitic rocks that are represented by serpentinites and talc- carbonates rocks and metabasalts, Island arc assemblage are represented by metasediments and metavolcanics rocks, syn orogenic granites, late orogenic granites, episyenite, dikes (aplitic and basaltic), and stream sediments. The common alteration features are generally represented by hematitization, sericitization, saussuritization, kaolinitization, albitization, chloritization, silicification, and muscovitization. Y/Ho, Zr/Hf, Nb/Ta, Ce/Ce*, Eu/Eu*and La/Y ratios indicated that the studied area was subjected to severe changes in the physic-chemical conditions leading to migration and sometimes accumulation of various elements. The presence of conjugated M-W type tetrad effect confirms the presence of these conditions and the clear relation of this phenomena with gold and silver mineralization in granites and pegmatites. Mineralogical investigations show the presence of fergusonite and columbite as Nb-Ta mineral group, uraninite, thorite, uranothorite and zircon thorite intergrowth as radioactive minerals, zircon, fluorite and allanite as radio- REEs bearing minerals, pyrite represent sulphides, in addition to apatite, garnet and natural brass.

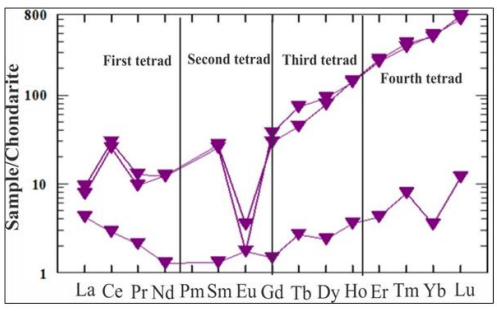

Fig. 14. *Chondrite normalized REE diagram (**Boynton, 1984**) for the investigated pegmatites. Symbols are the same as in Fig. 7.*

REFERENCES

[1] Abedini A, Calamari AA (2016). Geochemical characteristics of the Arabshah kaolin deposit, Takab geothermal field, NW Iran. Arabian Journal of Geosciences **9** (548): 1–16. doi: 10.1007/s12517-016-2572

[2] Abedini A, Rezaei Azizi M, Calagari AA, Cheshmehsari M (2017). Rare earth element geochemistry and tetrad effects of the Dalir phosphatic shales, northern Iran. Neues Jahrbuch für Geologie und Paläontologie – Abhandlungen **286**: 169–188. dio: 10.1127/njgpa/2017/0693

[3] Abedini A, Calagari AA, Rezaei Azizi M (2018). The tetrad-effect in rare earth elements distribution patterns of titanium-rich bauxites: Evidence from the Kanigorgeh deposit, NW Iran, Journal of Geochemical Exploration **186**: 129–142. dio: 10.1016/j.gexplo.2017.12.007

[4] Akagi T, Hashimoto Y, Fu FF, Tsuno H, Tao H, Nakano Y (2004). Variation of the distribution coefficients of rare earth elements in modern coral-lattices: Species and site dependencies. Geochimica et Cosmochimica Acta **68**: 2265–2273. dio: 10.1016/j.gca.2003.12.014

[5] Alexander P (2010). Mineralogy and geochemistry of the sodium metasomatism-related uranium occurrence of Aricheng South, Guyana. Miner. Deposita. **45**: 351–367. dio: 10.1007/s00126-010-0278-7

[6] Bau M (1996). Controls on the fractionation of isovalent trace elements in magmatic and aqueous systems: evidence from Y/Ho, Zr/Hf, and lanthanide tetrad effect. Contrib. Mineral. Petrol **123**: 323–333. dio: 10.1007/s004100050159

[7] Bau M (1997). The lanthanide tetrad effect in highly evolved felsic igneous rocks a reply to the comment by Y.Pan. Contributions to Mineralogy and Petrology **128**: 409–412. dio: 10.1007/s004100050318

[8] Cao MJ, Li GM, Qin KZ, Seitmuratova EY, Liu YS (2013). Major and trace element characteristics of apatites in granitoids from Central Kazakhstan. implications for petrogenesis and mineralization. Resour Geol **62**: 63–83. dio: 10.1111/j.1751-3928.2011.00180.x

[9] Cathelineau M (1987). U-Th-RRE mobility during albitization and quartz dissolution in granitoids: Evidence from southeast French Massif Central. Bull. Mineral **110**: 249–259. dio:10.3406/bulmi.1987.7984

[10] Censi P, Sortino F, Zuddas P, Saiano F, Brusca L, Chiavetta S, Falcone EE (2016). Rare earths behaviour during the deposition of volcanic sublimates. Journal of Volcanology and Geothermal Research **33**: 53–63. dio: 10.1016/j.jvolgeores.2016.11.015

[11] Cuney M, Friedrich M (1987). Physicochemical and crystal-chemical controls on accessory mineral paragenesis in granitoids: implications for uranium metallogenesis, Bull. Minéral **110**: 235–47. dio:10.3406/bulmi.1987.7983

[12] Deer WA, Howie RA, Zussman J (1992). An Introduction to the Rock Forming Minerals," 2nd ed., Longman, London, 696p.

[13] EL-Mansi MM (2000). Colouration of fluorite and its relation to radioactivity. Journal of Mineralogical Society of Egypt **12**: 93-106.

[14] El-Mezayen AM, El-Feky MG, Omar SA, Ibrahim SA (2015). Geochemistry and a composite M-type with W-type of REE tetrad effect in altered granites of Abu Furad area, Central Eastern Desert, Egypt. Greener Journal of Geology and Earth Sciences **3**(2): 013-029. dio: 10.15580/GJGES.2015.2.111915161

[15] El-Mezayen AM, EK Abu Zeid, WS Hosny, El-Feky MG, Omar SA, SA Taalab (2019). Geochemistry, mineralogy, and radioactivity of the Abu Furad area, Central Eastern Desert, Egypt. Acta Geochim **38** (2): 307–326. dio: 10.1007/s11631-018-0302-7

[16] El Mowafy AA, El Galy MM, El Feky MG, Said A F (2007). Radiometeric and mineralogical investigations on the uriniferous pegmatites at Gabal Um Adawi area, southeastern Sinai, Egypt. The **10th** International Mining, Petroleum, and Metallurgical Engineering Conference; Mining, Code No. M 26.

[17] Feng JL (2010). Behaviour of rare earth elements and yttrium in ferromanganese concretions, gibbsite spots, and the surrounding terra rossa over dolomite during chemical weathering. Chemical Geology **271**: 112–132. doi: 10.1016/j.chemgeo.2010.01.003

[18] Feng JL, Gao SP, Zhang JF (2011). Lanthanide tetrad effect in ferromanganese concretions and terra rossa overlying dolomite during weathering," Chemie der Erde-Geochemistry **71**: 349–362. doi: 10.1016/j.chemer.2011.06.001

[19] Feng JL, Zhao ZH, Chen F, Hu HP (2014). Rare earth elements in sinters from the geothermal waters (hot springs) on the Tibetan Plateau, China. Journal of Volcanology and Geothermal Research **287**: 1–11. doi: 0.1016/j.jvolgeores.2014.09.009

[20] Förster HJ (2006). Composition and origin of intermediate solid solutions in the system thorite-xenotime-zircon-coffinite. Lithos **88**: 35–55. doi: 10.1016/j.lithos.2005.08.003

[21] Gaafar I, Aboelkhair H (2014). Analysis of Geological and Geophysical Datasets for Radioelement Exploration in Kab Amiri Area, Central Eastern Desert, Egypt. The Open Geology Journal **8** (Suppl 1: M3) 53p. doi: 10.2174/1874262901408010034

[22] Harris NBW, Marriner GF (1980). Geochemistry and petrogenesis of a peralkaline granite complex from the Midian Mountains, Saudia Arabia. Lithos **13**: 325-337. doi:10.1016/0024-4937(80)90052-3

[23] Hermann AG (1970). Yttrium and lanthanides," In Handbook of Geochemistry. Wedepohl, K.H. (Editors), Springer-Verlag, Berlin. 57-71.

[24] Ibrahima ME, El-Kalioby BA, Aly GM, El-Tohamy AM, Watanabe K (2015). Altered granitic rocks, Nusab El Balgum Area, Southwestern Desert, Egypt. Mineralogical and geochemical aspects of REEs. Ore Geology Reviews **70**: 252–261. doi: 10.1016/j.oregeorev.2015.04.016

[25] Irber W (1999). The lanthanide tetrad effect and its correlation with K/Rb, Eu/Eu*, Sr/Eu, Y/Ho, and Zr/Hf of evolving peraluminous granite suites. Geochimica et Cosmochimica Acta **63**: 489–508. doi:10.1016/S0016-7037(99)00027-7

[26] Jahn BM, Wu F, Capdevila R, Martineau F, Zhao Z, Wang Y (2001). Highly evolved juvenile granites with tetrad REE patterns: the Woduhe and Baerzhe granites from the Great Xing'an Mountains in NE China. Lithos **59**: 171-198. doi: 10.1016/S0024-4937(01)00066-4

[27] Kawabe I, Ohta A, Ishii S, tokumura M, Miyauchi K (1999). REE partitioning between Fe-Mn oxyhydroxide precipitates and weakly acid NaCl solutions: convex tetrad effect and fractionation of Y and Sc from heavy lanthanides. Geochemical Journal **33**: 167–180. doi: 10.2343/geochemj.33.167

[28] Lee SG, Asahara Y, Tanaka T, Kim NH, Kim KH, Yi K, Masuda A, Song YS (2010). La–Ce and Sm–Nd isotopic systematics of early Proterozoic leucogranite with tetrad REE pattern. Chemical Geology, **276**: 360–373. doi: 10.1016/j.chemgeo.2010.07.003

[29] London D, (1987). Internal differentiation of rare-element pegmatites: effect of boron, phosphorus and fluorine. Geochim. Cosmochim. Acta **51**: 403– 420. doi: 10.1016/0016-7037(87)90058-5

[30] Mahdy AI, El-Kammar AM (2003). Geochemical Partitioning of Isovalent and Tetrad Effect of REE Associating Episynitization of Kab Amiri Granites, Central Eastern Desert of Egypt. pp.111–125. **5th** In. Comf. of Geology of Middle East Cairo Egypt.

[31] Manning DAC (1981). The effect of fluorine on liquidus phase relationship in the system Oz-Ab-Or with excess water at 1 kb. Contrib. Mineral. Petrol **76**: 206–215. doi: 10.1007/BF00371960

[32] Mason B, Moore CB (1991). Principles of Geochemistry. **4th** edition, Wiley Eastern Limited, 350 p.

[33] Masuda A, Kawakami O, Dohmoto Y, Takenaka T (1987). Lanthanide tetrad effects in nature: Two mutually opposite types W and M. Geochemical Journal **21**: 119–124. doi: 10.2343/geochemj.21.119

[34] Meyer C, Hemely JJ (1967). Wall rock alteration in geochemistry of Ore Deposits (ed. H.L. Barnes) [M]. pp.166–235. New York.

[35] Monecke T, Kempe U, Monecke J, Sala M, Wolf D (2002). Tetrad effect in rare earth element distribution patterns: a method of quantification with application to rock and mineral samples from granite-related rare metal deposits. Geochim Cosmochim Acta **66**: 1185–1196. doi: 10.1016/S0016-7037(01)00849-3

[36] Nasbitt HW, Young GM (1989). Formation and diagenesis of weathering profiles [J]. Journal of Geology **97**: 129−147. doi: doi.org/10.1086/629290

[37] Rezaei Azizi M, Abedini A, Alipour S, Niroomand S, Sasmaz A, Talaei B (2017). Rare earth element geochemistry and tetrad effects in fluorites: A case study from the Qahr-Abad deposit, Iran. Neues Jahrbuch für Geologie und Paläontologie –Abhandlungen **383**: 255–273. doi: 10.1127/njgpa/2017/0639

[38] Scott AW, Ricketts A (2000). Allanite-(Ce) From the Eocene Casto Granite, Idaho: Response to Hydrothermal Alteration. The Canadian Mineralogist **38**: 81-100. doi:10.2113/gscanmin.38.1.81

[39] Stemprok M (1979). Mineralized granites and their origin: review of MAWAM contributions. Episodes **12**: 49-53. doi: 10.18814/epiiugs/1979/v2i3/005

[40] Takahashi Y, Yoshida H, Sato N, Hama K, Yusa Y, Shimizu H (2002). W- and M-type tetrad effects in REE patterns for water–rock systems in the Tono uranium deposit, central Japan. Chemical Geology **184**: 311–335. doi: 10.1016/S0009-2541(01)00388-6

[41] Takahashia Y, Chatellier X, Hattorid KH, Kato K, Fortin D (2005). Adsorption of rare earth elements onto bacterial cell walls and its implication for REE sorption onto natural microbial mats. Chemical Geology **219**: 53–67. doi: 10.1016/j.chemgeo.2005.02.009

[42] Tang M, Wang XL, Shu XJ, Wang D, Yang T, Gopon P (2014). Hafnium isotopic heterogeneity in zircons from granitic rocks: Geochemical evaluation and modeling of "zircon effect" in crustal anatexis. Earth and Planetary Science Letters **389**: 188-199. to hydrothermal alteration. Can. Mineral. Mag. **38**: 81–100. doi: 10.1016/j.epsl.2013.12.036

[43] Tutlle OF, Bowen NL (1958). Origin of granite in the light of experimental studies in the system $NaAlSi_3O_8$- $KAlSi_3O_8$-SiO_3-H_2O [J]. Geol. Soc. Am. Mineral. 74: 153p.

[44] Watanabe Y, Sato R, Sulaksono A (2018). Role of Potassic Alteration for Porphyry Cu Mineralization: Implication for the Absence of Porphyry Cu Deposits in Japan. Resource Geology **68**: 195–207. doi: 10.1111/rge.12165

[45] Wood SA, Ricketts A (2000). Allanite-(Ce) from the Eocene Casto granite, Idaho: Response to hydrothermal alteration. The Canadian Mineralogist 38(1): 81-100. doi: 10.2113/gscanmin.38.1.81

[46] Zhang J, Amakawam H, Nozaki Y (1994). The comparative behaviors of yttrium and lanthanides in seawater of the North Pacific [J]. Geophys. Res. Lett. **21**: 2677–2680. doi: 10.1029/94GL02404

[47] Zhao ZH, Bao ZW, Lee SG (2008). A composite M- With W-type of REE tetrad effect in a north China alkaline complex. Geochim Cosmochim Acta **72**: 95-110. doi:10.1007/s11434-010-3231-3

[48] Zhao ZH, Bao Z, Qiao Y (2010). A peculiar composite M- and W-type REE tetrad effect: Evidence from the Shuiquangou alkaline syenite complex, Hebei Province, China. Chin Sci Bull **55**: 2684−2696. doi:10.1007/s11434-010-3231-3

[49] Zhang GL, Smith-Duque C (2014). Seafloor basalt alteration and chemical change in the ultra-thinly sedimented South Pacific. Geochemistry, Geophysics, Geosystem **15**: 066–3080. doi:10.1002/2013GC005141

Citation: *Sherif A. Taalab, et.al., " Mineralogical and Geochemical Studies on Kab Amiri Altered Granetic Rocks and Associated Pegmatite, Central Eastern Desert of Egypt", International Journal of Mining Science (IJMS), vol. 6, no. 2, pp. 11-33, 2020. Available: DOI: http://dx.doi.org/ 10.20431/ 2454-9428.0602002*